Pre-injection magnetotelluric surveys at the Aquistore CO_2 sequestration site, Estevan, Saskatchewan, Canada

Joe McLeod[a], Ian Ferguson[b,f], Jim Craven[c], Brian Roberts[d], Bernard Giroux[e]

a. University of Manitoba, Department Geological Sciences, Winnipeg, MB, Canada, R3T 2N2. joemcleodj@gmail.com
b. University of Manitoba, Department Geological Sciences, Winnipeg, MB, Canada, R3T 2N2. ij_ferguson@umanitoba.ca
c. Natural Resources Canada, 601 Booth St., Ottawa, ON, Canada, K1A 0E8. Jim.Craven@canada.ca
d. Natural Resources Canada, 601 Booth St., Ottawa, ON, Canada, K1A 0E8. Brian.Roberts@canada.ca
e. Institut Nationale de la Recherche Scientifique, Centre Eau Terre Environment, 490, rue de la Couronne Québec, Canada, G1K 9A9. bernard.giroux@ete.inrs.ca
f. Corresponding author. Phone 1-204-474-9154

ABSTRACT

Magnetotelluric (MT) soundings were conducted in a 4×4 km area at the Aquistore CO_2 sequestration site at Estevan, Saskatchewan, Canada in 2013, 2014 and 2015, prior to CO_2 injection. The MT response is locally one-dimensional but spatially variable at short periods (<0.003 s), regionally one-dimensional at intermediate periods (0.01 s to 10 s), and two-dimensional at long periods (>30 s). Responses corresponding to Williston Basin rocks are uniform across the area. A representative MT response was inverted using constraints derived from a resistivity well-log. Beneath the Jurassic Watrous to Vanguard formations (at depths greater than 1240-1600 m), the resistivity of the inversion model is consistently 20-30% lower than in the reference well-log model, consistent with the MT method sensing the longitudinal resistivity of the more strongly stratified units at these depths. Electromagnetic noise in the MT data set includes high-frequency odd harmonics of the 60 Hz source and a broad-band source, spatially associated with the CO_2 pipeline, observed only in 2014. Within the period range 10^{-4} to 10^2 s, but outside the bands influenced by the broad-band noise, the off-diagonal MT impedance response at Aquistore can be measured with an RMS repeatability of 1% or better.

KEYWORDS

Aquistore; CO_2 sequestration; pre-injection; geophysics; magnetotelluric

1. INTRODUCTION

The Aquistore project is a large-scale carbon dioxide (CO_2) capture and sequestration initiative, taking place to the southwest of Estevan, Saskatchewan. Emissions of CO_2 generated from SaskPower's Boundary Dam Power Station are captured and injected, in liquid form, deep into stable sedimentary packages of the Williston Basin for long-term storage (Rostron et al., 2014). The overall aim of the project is to reduce greenhouse gas emissions coming from a fixed source of CO_2 discharge, while demonstrating the effectiveness of using geological formations as a sequestration reservoir (Worth et al., 2014). The Aquistore reservoir is the Cambrian-Ordovician aquifer system of the Deadwood and Winnipeg Formations of the Williston basin. The 150 m thick reservoir is at 3400 m depth (Rostron et al., 2014). It is deep in comparison to the reservoir depth at a number of other CO_2 sequestration site studies, e.g., 650 m at the Ketzin site in Germany (Bergmann et al., 2012), 1100 m at the Kevin Dome site in the United States (Zhdanov et al., 2013), and 1500 m at the Hontomín site in Spain (Ogaya et al., 2016) but it is comparable to the 3300 m reservoir depth at the Cranfield site in the United States (Hovorka et al. 2011). The surface environment in the study area includes a number of sources of electromagnetic noise including infrastructure of the Boundary Dam Power Station and prairie farming operations. Such noise creates potential challenges for both controlled and natural source electromagnetic measurements (Ferguson, 2012; Escalas et al., 2013).

Natural and controlled-source electromagnetic monitoring can provide valuable constraints on changes in fluid content and fluid salinity in the sub-surface and time-lapse natural and controlled-source electromagnetic surveys will be used to monitor subsurface changes in electrical conductivity in the future. Dissolution of injected CO_2 in pore water can have a strong effect on the electrical resistivity of the water and the rock (e.g., Börner et al., 2013; Börner et al., 2015; Bosch et al., 2015). The presence of undissolved CO_2 in gaseous form will increase the resistivity of the pore fluids and the bulk rock. However, the reactive nature of CO_2 means that it will dissolve into the pore waters in large amounts. In this state its effect on the electrical resistivity of the pore fluid depends in a complicated way on the CO_2 concentration, pore fluid salinity, temperature and pressure (Börner et al., 2015). Laboratory studies show that in low salinity fluids, the dissolved ions from the dissociation of carbonic acid will increase the pore water conductivity, but in highly saline fluids, the dissolved CO_2 may decrease the conductivity because of increased ionic interactions and decreased ionic mobility (Börner et al., 2015). This situation may apply at the Aquistore site where the salinity of the reservoir is of order 300,000 ppm (e.g., Roach et al., 2015). Resistivity results from electromagnetic monitoring can be integrated effectively with other geophysical parameters such as seismic velocity (e.g., Bergmann et al., 2014; Ogaya et al., 2016) and has potential to be directly integrated into the determination of hydrogeological properties (e.g., Commer et al., 2015; Kirkby et al., 2016).

The main natural-source electromagnetic method used for imaging deeper CO_2 sequestration reservoirs is the magnetotelluric (MT) method (Chave & Jones, 2012). This study focuses on the use of MT soundings prior to the commencement of CO_2 injection at the Aquistore site. Pre-injection MT soundings were conducted in 2013, 2014 and 2015 over a 4×4 km area surrounding the Aquistore injection well (Fig. 1). The four objectives of the study are: to characterize the MT response at the Aquistore injection site; to define the background electrical resistivity structure around the Aquistore site; to examine the effects of the noise on surface electromagnetic measurements; and to use the derived resistivity model to conduct preliminary examination of the sensitivity of surface electromagnetic measurements to resistivity changes associated with the injection of CO_2 into the reservoir and leakage into the overlying strata.

Pre-injection MT surveys form part of the Natural Resources Canada (NRCan) Integrated CO_2 Measurement, Monitoring & Verification Study, which was formulated to simultaneously test and calibrate monitoring tools at the injection site. The injection of CO_2 at the Aquistore site will be dependent on the integrity of the sealing units and on the subsurface distribution of the fluid. A suite of monitoring techniques is being used at the site to ensure that these requirements are being satisfied at multiple stages of the injection (Worth et al., 2014). The most extensive studies involve seismic methods (White et al., 2014) but other less intensive monitoring methods are desirable to either complement or substitute for seismic methods. Ultimately, the observations will be integrated quantitatively to estimate the subsurface distribution of CO_2 and ground deformation that may affect the integrity of the storage complex.

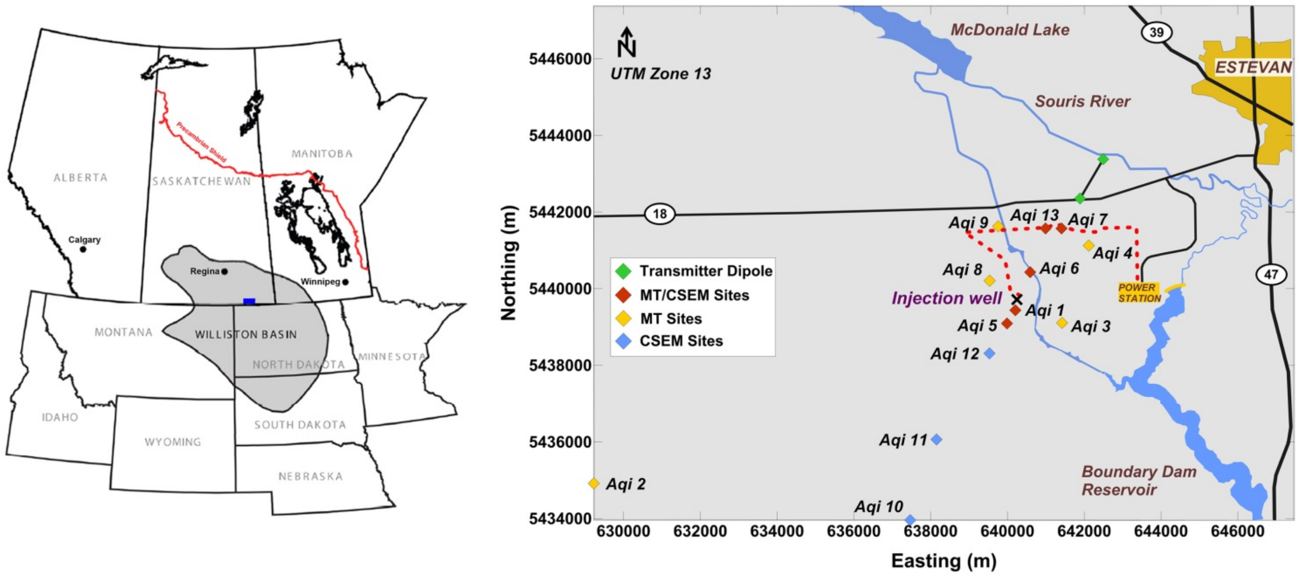

Figure 1. Aquistore surface electromagnetic survey area. Left panel shows the site location (blue rectangle) within the Williston Basin (modified from Rostron et al., 2014). Right panel shows the location of the surface electromagnetic survey sites from 2013-2015 and other important features. Yellow diamonds show MT sites and blue diamonds show sites used for controlled-source electromagnetic soundings in 2013 and 2015 as well as MT sites in 2014 and 2015. Site aqi02 was the MT remote reference site for the 2013 survey and part of the 2014 survey and a second MT remote reference site aqi15 was located 16 km northeast of Estevan (at UTM 13U 5458500N 657500E) was used in part of the 2014 survey and the 2015 survey. Solid black lines are roads and dashed red line is the CO_2 pipeline from the power station to the injection well. The southern limit of the map is 49° 2' N, 4 km north of the Canada-United States border.

The NRCan pre-injection electromagnetic study also included surface controlled-source measurements using a 1 km long, 30 A electric bipole source. Recordings of the radial electric field component were made in 2013 and 2015 surveys along an inline receiver profile at offsets up to 9.5 km. Preliminary evaluation of the acquired data sets indicates that the transmitted signals are observable at all of the profile locations (McLeod, 2016) and the resulting data set is currently under analysis. The results of the full analysis of the controlled-source electromagnetic data set along with a more extensive examination of the sensitivity of the response will be published in a subsequent paper.

A further component of controlled-source electromagnetic investigations at Aquistore includes a survey by British Petroleum (BP) and GroundMetrics, Inc. (GMI) using a novel borehole to surface electromagnetic (BSEM) survey configuration (Hibbs, 2013). This method injects an electric current using a surface array of electrodes oriented radially to the well. Surface measurements recording the distribution of electric current returning from reservoir depths via the injection well casing provides a means to detect signals from reservoir depths. The data from the BSEM survey have been analyzed independently of the present study and only limited information from that study has been made publicly available. Daley et al. (2014) describe modelling of the theoretical response of a borehole-source electromagnetic system at Aquistore.

Relatively few electromagnetic measurements have been made in association with CO_2 storage projects. Examples of onshore sites at which surface electromagnetic methods have been applied or modelled include proposed CO_2 sites at Kevin Dome in the United States (Zhdanov et al., 2013), Ketzin in Germany (Streich et al., 2010, 2011, 2013; Grayver et al., 2013) and Hontomín in Spain (Ogaya et al., 2013; Vilamajó et al., 2013; Ogaya et al., 2014; Vilamajó et al., 2015; Ogaya et al. 2016). Cross-hole electrical resistivity tomography has been applied at sequestration sites instrumented with downhole electrodes e.g., at Ketzin in Germany (Bergmann et al., 2012) and Cranfield in the United States (Commer et al., 2016). Other studies have examined the theoretical electromagnetic or electrical response of planned or hypothetical land sequestration sites (e.g., Gasperikova & Hoverston, 2006; Wirianto et al., 2010; Bouchedda & Giroux, 2016) and off-shore sequestration sites (e.g., Bhuyian et al., 2012; Eliasson et al., 2014; Kang et al., 2015).

There have also been a number of studies that have examined the time-variations in MT responses. These studies have been motivated by the potential use of MT studies in earthquake prediction (e.g., Auld et al., 1992; Eisel & Egbert, 2001; Hanekop & Simpson, 2006; Chiang et al., 2008), volcano monitoring (e.g., Wawrzyniak et al., 2017; Ladanivskyy et al., 2017) hydraulic fracturing (e.g., He et al., 2012; Peacock et al., 2013; Rosas-Carbajal et al., 2015; Thiel, 2017; Abdelfettah et al., 2018) and for monitoring temporal changes in other targets (e.g., Rees et al. 2016).

2. GEOLOGICAL SETTING

2.1 Precambrian basement

The Williston Basin is a large intracratonic sedimentary basin that extends from southern Saskatchewan and southwest Manitoba into Montana and South Dakota (Fig. 1). It lies unconformably on Archean and Proterozoic-age basement and is centered on the Proterozoic Trans Hudson Orogen (Fowler and Nisbet, 1984). The current geometry of the Precambrian terranes was established around 1.95 – 1.75 Ga when convergent tectonics in the Trans-Hudson orogen (THO) welded together the Archean Superior, Wyoming and Hearn/Rae cratons to form part of Laurentia (e.g., Ansdell, 2005). Archean rocks exposed in, and present beneath, the central Trans Hudson orogen are interpreted to form part of a buried craton known as the Sask Craton. The study area lies near the western margin of this craton.

2.2 Williston Basin

The Williston basin formed by subsidence throughout much of the Phanerozoic about a depo-centre in North Dakota (Fig. 1). The basin is presently interpreted to have formed during episodic subsidence (Zhu and Hajnal, 1993; Osadetz et al., 2002). In east-central Saskatchewan, the basin thickness is between 2.2 and 3 km (Whittaker and Worth, 2011) and ages of the constituent strata range from middle Cambrian to early Cenozoic. The rocks dip gently to the southwest.

In a broad classification, the rocks of the Williston Basin can be divided into three units: a basal clastic unit, a carbonate and evaporite dominated unit, and an upper clastic unit (Bachu, 2002; Vigrass et al., 2007). In terms of depositional history, this classification is well-described by sequences of sediment accumulation corresponding to changes in sea level. The oldest rocks present in the Williston basin in the study area are the sandstones of the Cambrian Deadwood formation. These rocks are interpreted to form part of the Middle Cambrian to Upper Ordovician Sauk sequence (Rickets, 1989). The basal unit of the overlying Tippecanoe sequence of Middle Ordovician clastics and Upper Ordovician and Silurian carbonates is the Winnipeg Formation (LeFever et al., 1987; Osadetz et al., 2002). It consists of sandstone and shale (Whittaker and Worth, 2011). Deposition of the overlying Middle Devonian-Carboniferous Kaskasia sequence, is dominated by carbonates, evaporites and shale (Rickets, 1989). The Triassic shales of the succeeding Lower Watrous Formation are unconformably overlain by the Jurassic evaporites of the Upper Watrous Formation. These units may be part of the Absaroka sequence

(Rickets, 1989) but they are sometimes included Zuni sequence (Zhu & Hajnal, 1993). The rocks are overlain unconformably by a Jurassic to Paleocene Zuni succession (Osadetz et al., 2002) dominated by shales. It is in turn overlain unconformably by Pleistocene deposits.

The Aquistore reservoir is the aquifer system of the Deadwood and Winnipeg Formations. The Deadwood formation lies unconformably on the Precambrian basement. In the study area, it is predominantly a sandstone layer but interbeds of silty and shaly rocks in the Deadwood add heterogeneity (Whittaker and Worth, 2011). The beds of the formation show an upward coarsening character (Dixon, 2008). The Winnipeg Formation is predominantly a sandstone unit. Subdivisions of the formation in the study area are the Black Island and Icebox members (Smith and Bend, 2004; Whittaker and Worth, 2011). The Black Island unit is the lowest member in the formation and consists of well to poorly-sorted quartzose sandstone. Lying conformably on the Black Island sandstones are the shales of the Icebox member. These shales have been interpreted as an extensive flooding surface (Smith and Bend, 2004). At the Aquistore site, the Icebox member will serve as the primary seal for the injected fluid (Whittaker and Worth, 2011).

2.3 Surficial geology

The Tertiary Ravenscrag Formation, which extends to depths of 180 m beneath the surface, is the shallowest recognized geological unit in the Estevan area. Its lithology varies between sand, silt, clay, and lignite compositions (Irvine, 1978; Klappstein and Rostron, 2014). Seams of lignite coal embedded in these Tertiary deposits include the Estevan seam and the Boundary seam. The Estevan seam is the shallower of the two, and has been strip-mined in the area. Thin sequences of glacial till material unconformably overlie the Ravenscrag Formation. This overburden has a maximum thickness of 10 m in the Aquistore region. Where strip mining is significant, mine spoil sits in place of the typical glacial overburden (Klappstein and Rostron, 2014). In some locations in the Estevan area, buried channel aquifers are present beneath the till (Klappstein and Rostron, 2014).

3. ELECTROMAGNETIC SETTING

3.1 The magnetotelluric method

The MT method uses time-series surface measurements of natural electric and magnetic fields to derive sub-surface resistivity information (e.g., Vozoff, 1991; Chave & Jones, 2012). Recordings from a second site, a remote-reference site, are used to remove the effects of any noise that is incoherent between the main and remote sites (Gamble et al., 1979). Spectral analysis is performed on the different vector components of the fields to estimate a frequency-domain MT impedance **Z**(ω). The tensor impedance defines the linear relationship in the frequency domain of vector electric field **E**(ω) (which is the secondary field, the response of the sub-surface) and the vector magnetic field **H**(ω) (which contains the primary field, the source of the signal). It is defined:

$$\mathbf{E}(\omega) = \mathbf{Z}(\omega)\mathbf{H}(\omega) \qquad \text{Eq. 1}$$

where, in the normal measurement system with north being the *x*-direction, east being the *y*-direction (and *z* being vertical downwards),

$$\mathbf{E} = \begin{bmatrix} E_x(\omega) \\ E_y(\omega) \end{bmatrix} \quad \mathbf{H} = \begin{bmatrix} H_x(\omega) \\ H_y(\omega) \end{bmatrix} \quad \mathbf{Z} = \begin{bmatrix} Z_{xx}(\omega) & Z_{xy}(\omega) \\ Z_{yx}(\omega) & Z_{yy}(\omega) \end{bmatrix} \qquad \text{Eq. 2}$$

Depth information is obtained from period-dependence of the MT impedance response: short period (high-frequency) results correspond to small skin-depths (the depth at which the primary field decays to 1/e) and near-surface structure and long period (low-frequency) values correspond to large skin-depths and deep structure. Both the phase and magnitude of the impedance are related to the underlying resistivity structure. The impedance magnitude is usually examined in terms of the equivalent apparent resistivity which will equal the true resistivity over a uniform structure, and a weighted-average value over the penetration depth of the signals in a layered or 1-D structure. For a layered earth structure the impedance phase is between 0^{o} and 45^{o} at periods for which apparent resistivity is increasing with period (corresponding to structures becoming more resistive with depth) and it is between 45^{o} and 90^{o} at periods for which the apparent resistivity is decreasing with period (structure becoming more conductive with depth).

In 2-D and 3-D structures the apparent resistivity and phase become azimuthally-dependent quantities.

The four-component complex-valued MT impedance tensor can be used to estimate the dimensionality of the response. For 2-D or approximately 2-D structures it can be used to estimate the geoelectric strike direction. In this case, after rotation of the coordinate system to align with the strike direction, the impedance response becomes:

$$\mathbf{Z}(\omega) == \begin{bmatrix} 0 & Z_{\mathrm{TE}}(\omega) \\ -Z_{\mathrm{TM}}(\omega) & 0 \end{bmatrix} \qquad \text{Eq. 3}$$

The off-diagonal impedance mode corresponding to electric current flow parallel to strike is called the transverse electric (TE) mode and the off-diagonal mode corresponding to electric current flow perpendicular to strike is called the transverse magnetic (TM) mode.

3.2 Large-scale resistivity structures

Much of the information on the electrical resistivity structure of the Williston Basin has been derived from well-logs and from MT surveys. Jones (1988) provides a synthesis of Laterolog resistivity log results for a profile crossing the central Williston Basin at 49^{o} 20’ N, crossing approximately 25 km north of the Aquistore MT survey area (Fig. 2). The large-scale responses reflect the geological structure. Clastic-dominated rocks of the basal Sauk and Tippecanoe sequences, including the Deadwood and Winnipeg Formations, form a relatively conductive (<30 Ω.m) basal layer. This layer becomes significantly more conductive towards the east of the basin (Gowan et al., 2009) because of increased salinity in the Cambrian-Ordovician aquifer system (Ferguson et al., 2007). The Devonian-Mississippian Kaskasia sequence, which is dominated by carbonates, evaporites and shale, forms a more resistive layer that is ~1000 m thick near the Aquistore location (Fig. 2). The dominantly clastic rocks of the Zuni sequence in the uppermost 1200 m of the central Williston Basin are very conductive (<10 Ω.m). The electromagnetic masking effect of these rocks will limit the resolution of the MT method at greater depths.

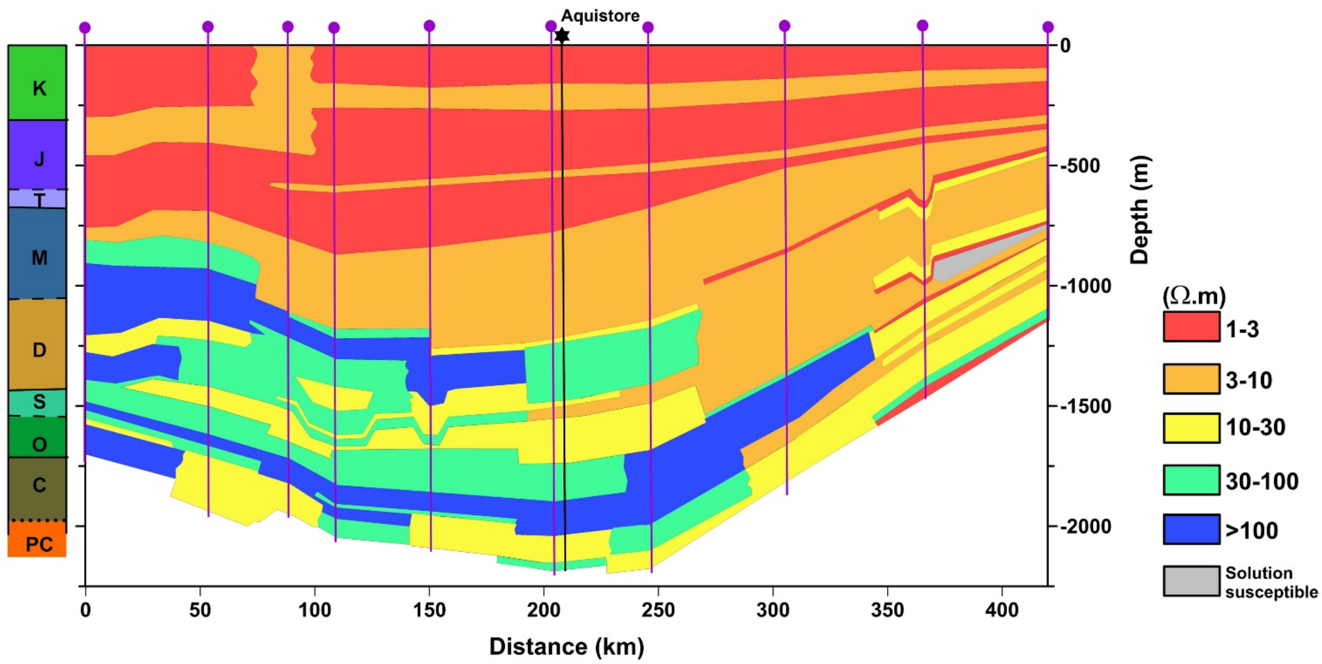

Figure 2. Large scale resistivity structure along a 420 km west-east profile across the Williston Basin at 49^{o} 20' N between 105^{o} 46' W and 100^{o} W synthesized from well logs (modified from Jones 1988). Results are shown for depths below the top of the Lower Cretaceous (Colorado Group) rocks. Coloured rectangles at left show the age (PC=Precambrian, C=Cambrian, O=Ordovician, S=Silurian, D=Devonian M=Mississippian, T=Triassic, J=Jurassic, K=Cretaceous). See Fig. 3 for the actual geological units. Vertical purple lines show location of logs used to define the resistivity. The Aquistore well is shown by the black vertical line. The Aquistore reservoir is at the base of the basin and underlies a thick sequence of conductive sedimentary rocks including 1400 m of <10 Ω.m rocks.

Many of the MT field studies conducted in the Williston Basin have targeted structures in the Precambrian crust and mantle but still provide some information on the resistivity structure of the basin. Unconstrained 1-D inversions of MT data from the central and eastern Williston Basin model yield an uppermost layer with a base corresponding to the depth of the top of the Lower Paleozoic sedimentary rocks, reflecting the higher conductivity of the overlying Upper Paleozoic and Mesozoic sedimentary rocks (Rankin & Kao, 1978; Jones & Savage, 1986; Jones & Craven, 1990). With the introduction of inversion constraints or starting models based on resistivity well-logs the MT response of the Williston Basin rocks can be better represented by a three-layer model. Maidens & Paulen (1988) conducted 1-D inversions of MT responses from 200 km west of the current study area and determined a three-layer representation of the Williston Basin rocks with the layers corresponding closely with the Cambrian to Middle Devonian, Mississippian to Late Devonian, and Cretaceous sedimentary rocks. Jones (1988) used a more detailed resistivity model derived from well logs (Fig. 2) to define the static shift component of galvanic distortion at sites in the southern Williston Basin. Gowan et al. (2009) conducted a detailed comparison of well log and MT responses at sites in the eastern Williston Basin and found it was necessary to combine the two data sets in order to define a comprehensive resistivity model. The MT data provide resolution of the near-surface and basement resistivity structure outside the depth range of the well-logs whereas the well-logs provide detailed information on the internal resistivity structure in the sedimentary rocks that cannot be resolved by the MT method.

The primary focus of previous MT studies in the Williston Basin has been the North American Central Plains (NACP) conductor which is a continental-scale electrical conductivity anomaly within the underlying Precambrian crust (Jones & Craven, 1990; Jones, 1993; Jones et al., 1993; Jones et al., 1997; Jones et al., 2005; and references therein). The structure of the NACP in southern Saskatchewan was investigated in detail in the COPROD2 modelling study in which a number of different scientific groups conducted 2-D MT inversions of MT data from a profile extending past the Aquistore site (Jones, 1993). In more recent findings, the NACP is interpreted to lie at mid-crustal depths on the western flank of the Sask craton and to been formed by the metamorphic and structural processes associated with the convergence of juvenile Proterozoic rocks onto the Sask craton margin (Jones et al., 2005; Gowan et al., 2009).

In the southern Williston Basin in Canada the NACP has an approximately north-south trend so the TE response corresponds to the approximately north-south electric currents (and the Z_{xy} impedance component), and the TM response to east-west currents (and the Z_{yx} impedance component). The NACP conductor causes a separation of the TE and TM apparent resistivity and phase responses at long periods, due to the decrease in TE apparent resistivity and increase in TE phase associated with the enhanced conductivity. The strength of this effect increases with proximity to the NACP conductor and the period of its onset of decreases with proximity to the conductor, to a minimum period of 20 s in the phase response at sites above the conductor. At sites near the conductor there are also some corresponding effects in the longer period TM response (Jones, 1993). The Aquistore site lies above the eastern margin of the NACP conductor and the effects of the conductor are therefore expected to be observed in long period MT data collected in the Aquistore project.

3.3 Resistivity structure at the Aquifer site

Detailed information on the resistivity structure beneath the Aquistore site is available from well-log measurements in the Aquistore injection well. Figure 3 shows resistivity data derived from the Schlumberger AHF90 four-foot array induction log resampled at 3 m intervals. A simplified 16-layer resistivity model is also shown and the corresponding lithological units and resistivity values are listed in Table 1. The simplified model was obtained using a visually estimated fit to the well-log data in log-resistivity space. This model was used as a reference resistivity model in the present study. As is to be expected, at a coarse scale the Aquistore resistivity well-log data resemble the synthesized well-log data shown in Fig. 2.

For future monitoring applications using MT, it is critical to be able to accurately relate the MT responses to well-log resistivity information. As noted in Gowan et al. (2009) the MT responses may be influenced by the structure above and below the depth range of the well-log data and several additional factors may contribute to differences between the resistivity derived using MT data and well-log methods: residual effects of drilling-fluid invasion in the well-log data; lateral variations in the rocks e.g., associated with facies change; and the different inherent sampling of small-scale structures in the rocks by the MT and well-log measurements.

The effect of stratification can be assessed by calculating the coefficient of anisotropy for layers in the simplified resistivity model (e.g., Maillet, 1947). This calculation was done for the vertical transverse isotropy in which resistivity is identical in all horizontal directions, i.e., parallel to the bedding plane. The coefficient of anisotropy is (e.g., Edwards et al., 1988):

$$\lambda = \left(\frac{\rho_{\perp}}{\rho_{//}}\right)^{1/2} = \left[\frac{\sum(h_i\rho_i)\sum(h_i/\rho_i)}{\left(\sum h_i\right)^2}\right]^{1/2} \qquad \text{Eq. 4}$$

where $\rho_{\perp}$ and $\rho_{//}$ are the resistivity sensed by electric currents flowing perpendicular and parallel to the bedding and h_i and ρ_i are the thickness and resistivity of the individual layers. Results shown in Fig. 3 and Table 1 are based on the 3 m re-sampled resistivity data that do not account for smaller-scale layering. The coefficient of anisotropy is moderate to high in Cambrian to Ordovician units (>2.5) reaching a value of 5.85 in the Deadwood and Winnipeg Formations. It is moderate (2-3) in Devonian and Mississippian units and low (<1.35) in Triassic and younger units.

The significant anisotropy of the Lower Paleozoic rocks means the resistivity values listed in Table 1 will be higher than the resistivity values that will be determined by the MT method. In a horizontally stratified structure, the MT method is based on horizontally-flowing electric currents, and therefore senses the longitudinal resistivity of the units. In the case of an internally-layered unit, it will yield a resistivity value for the unit equal to the inverse of the averaged conductivity of the sub-layers. This value is lower than the resistivity value estimated from geometrical averaging of the sub-layer resistivity values, the approach applied in the formulation of the simplified resistivity model. It is important to note that other electromagnetic methods, such as surface controlled-source electromagnetic measurements or well-log resistivity measurements, will generate vertically flowing currents and will therefore sense the resistivity of an internally-layered unit in a different way from MT measurements.

4. PRE-INJECTION MT SURVEYS

The distribution of surface electromagnetic sites in the pre-injection MT surveys was designed to provide MT responses in a 4x4 km area surrounding the injection well and controlled-source electromagnetic responses along an approximately NNE profile (exact azimuth magnetic N22˚E) crossing the injection well (Fig. 1). Modelling studies suggested the CO_2 injection plume may extend dominantly up-dip so the MT study area was offset from the injection well in the northeast direction and the controlled-source electromagnetic profile was installed approximately parallel to dip. Sites on the controlled-source profile extended to a distance of up to 6 km from the injection well and were also used for MT recordings in 2014 and 2015. A MT remote-reference site (aqi02) was located 10 km to the southwest of the injection well and used in the 2013 survey and part of the 2014 survey. A second, more-distant MT remote reference site (aqi15) was installed in second part of the 2014 survey and in the 2015 survey to the northeast of Estevan (not pictured in Fig. 1). The exact location of each MT and controlled-source electromagnetic site depended on logistical aspects including accessibility and site security, and on the necessity for the recordings to be an appropriate distance from infrastructure including buildings, powerlines, and fences (McLeod, 2016).

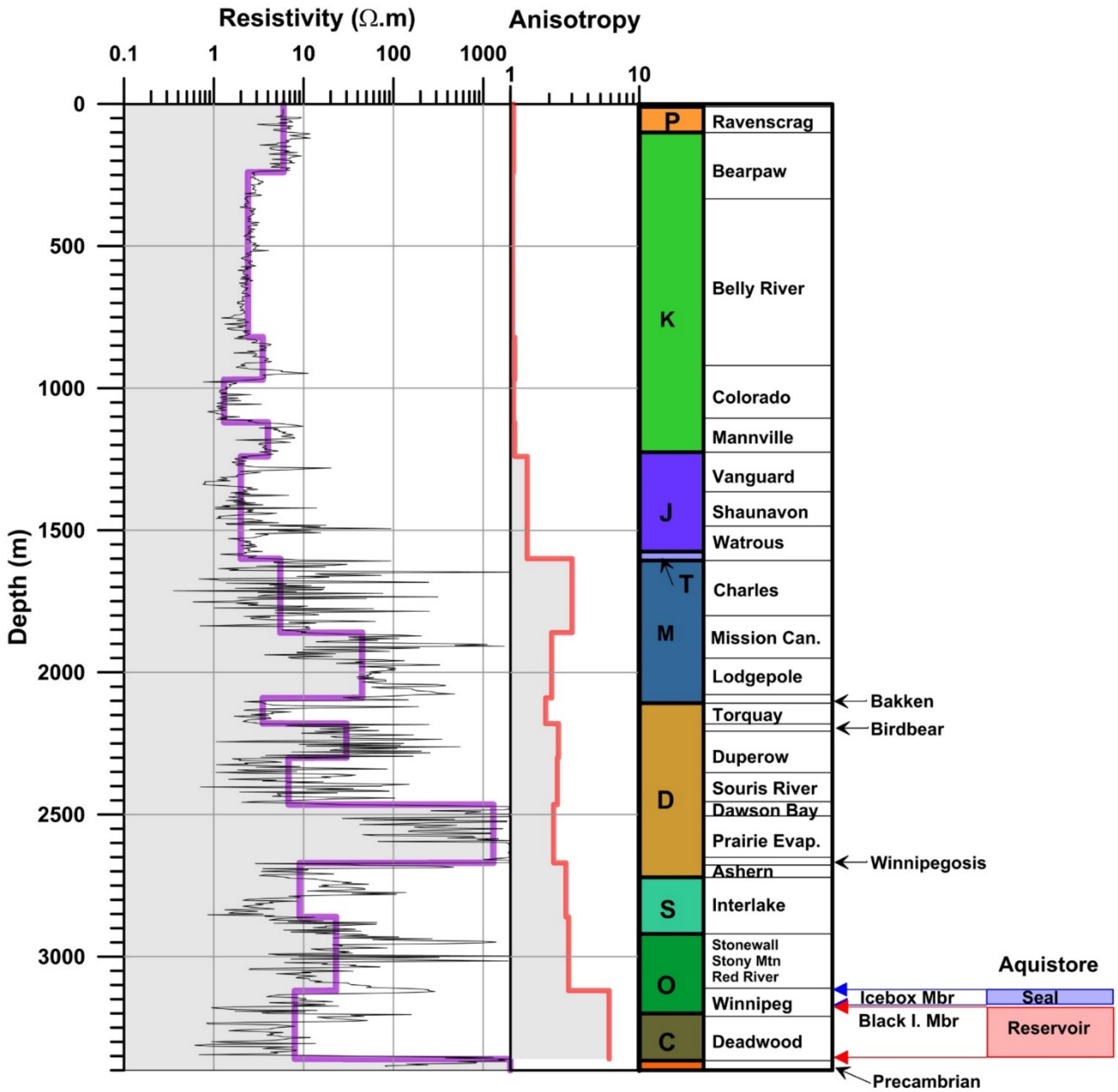

Figure 3. Resistivity section at the Aquifer site derived from 3 m resampling of four foot array induction log response (grey curve) and a manually fitted simplified 16-layer resistivity model (purple curve). The figure also shows the coefficient of anisotropy calculated for each layer of the simplified model using the 3 m resampled data. Coloured rectangles show the age (C=Cambrian, O=Ordovician, S=Silurian, D=Devonian M=Mississippian, T=Triassic, J=Jurassic, K=Cretaceous, P=Paleocene). The stratigraphic column includes only the thicker units and the labelled names include both formation and group names. “Shaunavon” includes both the Shaunavon and Gravelbourg formations.

Table 1: Parameters of simplified layered resistivity model

Layer	Thickness (m)	Resistivity (Ω.m)	Coefficient anisotropy	Main geological formations
1	240	6	1.06	Quaternary, Ravenscrag, Bearpaw
2	580	2.4	1.04	Belly River
3	150	3.5	1.08	Belly River-Colorado
4	150	1.3	1.06	Colorado
5	120	4	1.08	Mannville
6	360	2	1.35	Vanguard, Shaunavon, Gravelbourg, Watrous
7	260	5.5	3.01	Charles
8	230	45	2.09	Mission Canyon, Lodgepole
9	90	3.5	1.88	Bakken, Torquay
10	120	30	2.36	Birdbear, Duperow
11	165	6.8	2.32	Souris River
12	205	1300	2.17	Dawson Bay, Prairie Evaporite
13	190	9	2.70	Winnipegosis, Ashern, Interlake
14	260	23	2.83	Stonewall, Stony Mountain, Red River
15	240	8	5.85	Winnipeg-Deadwood
16	-	1000	-	Precambrian

As a way of expediting MT data collection, a deployment scheme was used in which the electric field was measured at every site and the more spatially-uniform magnetic field measured at a smaller number of representative sites. This procedure was enabled by the relatively close spacing of the recording sites and permitted an increased number of sites to be collected using the limited number of MT coils and time available. In order to obtain responses over desired period range, separate audio frequency MT (AMT) and broadband MT (here denoted by just “MT”) magnetic recordings were needed. Ideally AMT period magnetic data were imported from sites less than 1 km from the main site, and MT period data from sites less than 4 km away. It was possible to use AMT electric field recordings in both AMT and MT data processing.

It is useful to note the proximity of the MT sites to infrastructure at the Aquistore site (Fig. 1). All three MT surveys were completed after the installation in 2012 of the injection well, and the observation well 150 m to the north (Worth et al., 2014). The east-west part of the CO_2 pipeline, which is also used to transport CO_2 to the Weyburn area for enhanced oil recovery use, was under construction during the 2013 MT survey. The installation of the pipeline to the injection well was completed by July 2014 (Pipeline News, July 2014) prior to the 2014 MT survey. Initial CO_2 injection began in April 2015 but full-scale injection did not start until after the 2015 MT survey. As of February 2017, total CO_2 injection at Aquistore passed 100,000 tonnes.

The 2013 MT survey was conducted between 21^{st} and 26^{th} August 2013 at 12 recording sites, the 2014 survey was conducted between 6^{th} and 11^{th} November 2014 at 14 sites, and the 2015 survey between 2^{nd} and 6^{th} November 2015 at 7 sites (McLeod, 2016). MT data were recorded using Phoenix Geophysics MTU instrumentation. Telluric fields were recorded with 25 to 50 m dipole lines using porous pot electrodes, and magnetic fields were recorded with MT and AMT induction coil sensors. The AMT and MT recordings at each site were made for two or three nights for a typical total recording duration of 14.5 to 20 hours. The Phoenix MT equipment acquires data at different sampling rates: for the Aquistore survey an AMT sampling configuration was employed for almost all of the recordings providing discontinuous time series at 24,000 Hz and 2400 Hz sampling rates, and continuous time series at 150 Hz sampling rate.

Optimization of field procedures and understanding of the electromagnetic noise distribution across the Aquistore site increased considerably between each survey. For example, it was necessary to relocate several sites from the 2013 survey that were determined to be very noisy. Because of the limited availability of low noise magnetic field recordings in the 2013 survey the MT response was often obtained using local rather than remote reference processing. The results are based on the local electric field and lower noise magnetic field data imported from a quiet site such as aqi02. As will be discussed below, the 2014 survey results were also severely impacted by strong widely-distributed electromagnetic noise, and one outcome was the need to establish a more distant remote-reference station. Despite several limitations in the resulting MT data sets, the results allow all survey objectives to be achieved: defining the MT response at the Aquistore site; defining background electrical resistivity structure; examining the effects of the noise on surface electromagnetic measurements; and using the derived resistivity model to examine the sensitivity of surface electromagnetic measurements to sub-surface resistivity changes.

5. MT RESPONSE CHARACTERIZATION

5.1 Data processing

The MT data were processed using a Phoenix Geophysics software package which implements a robust cascade decimation code. The processing transforms the recorded time series into period-dependent MT impedance, apparent resistivity, and phase responses. The processing of the Aquistore MT data used fairly standard parameters as follows. Fourier transforms were computed at 4 frequencies per octave. For the robust processing, the time series were divided into 20 equal length segments for each recording interval from which crosspowers were calculated at the selected frequencies. Crosspowers were rejected if the coherency between the local and remote data was below a threshold of 0.35, or if the coherency between the telluric and magnetic data was below 0.25. The final responses were weighted based on their variance. The differences in AMT and MT coil responses leads to less reliable crosspower estimates at periods of >0.1 s for the AMT coils and <0.01 s for the MT coils. There is sufficient overlap in the two types of results that final combined responses for most sites are defined over a broad range of periods (10^{-4} s to $>10^{3}$ s).

5.2 MT responses

Figure 4 shows an example of the final MT response from aqi05, from the 2013 survey. The form of the response is very similar to that for most other stations in the Aquistore study area. The response is very close to 1-D at periods < 20 s with the off-diagonal Z_{xy} and Z_{yx} impedance response being almost identical and the magnitude of the diagonal Z_{xx} and Z_{yy} impedance components being much smaller than the magnitude of off-diagonal terms. This shorter period range defines the characteristic MT response of the Williston Basin sedimentary rocks. The variation of apparent resistivity and phase with period reflects varying resistivity with depth in the basin. In particular, the very conductive responses indicated by the high phase values at 0.1 to 10 s period and low apparent resistivity values at 1 to 10 s period can be attributed in large part to the conductive rocks noted at depths between 200 m and 1600 m in the well-log. There is also a contribution from the more resistive underlying Paleozoic rocks but the response of these rocks is masked by the overlying conductive sequence. At periods > 20 s the MT response at aqi05 indicates a two-dimensional structure with a north-south strike. The Z_{xy} and Z_{yx} responses diverge, with the Z_{xy} response exhibiting lower apparent resistivity and high phase as expected for a structure that is more conductive in the north-south direction. The Z_{xx} and Z_{yy} impedance components are still much smaller than the off-diagonal components indicating a low level of three-dimensionality in the response. This long period range defines the characteristic MT response of the NACP conductor.

The MT response at aqi5 shows a number of features that can be attributed to electromagnetic noise including increased variance of the diagonal impedance components. These noise features are strongest between periods of about 0.1 s and 10 s. This period distribution is likely a result of the combined effects of broader-band noise and lower signal levels in the MT dead-band (Viljanen, 2012). There is a clear decrease in the coherence of orthogonal electric and magnetic field components (E_x-H_y and E_y-H_x) in the same period range reflecting the decreased signal to noise ratio. The noise effects are much stronger in the raw data, prior to processing to remove crosspower estimates with the largest noise effects.

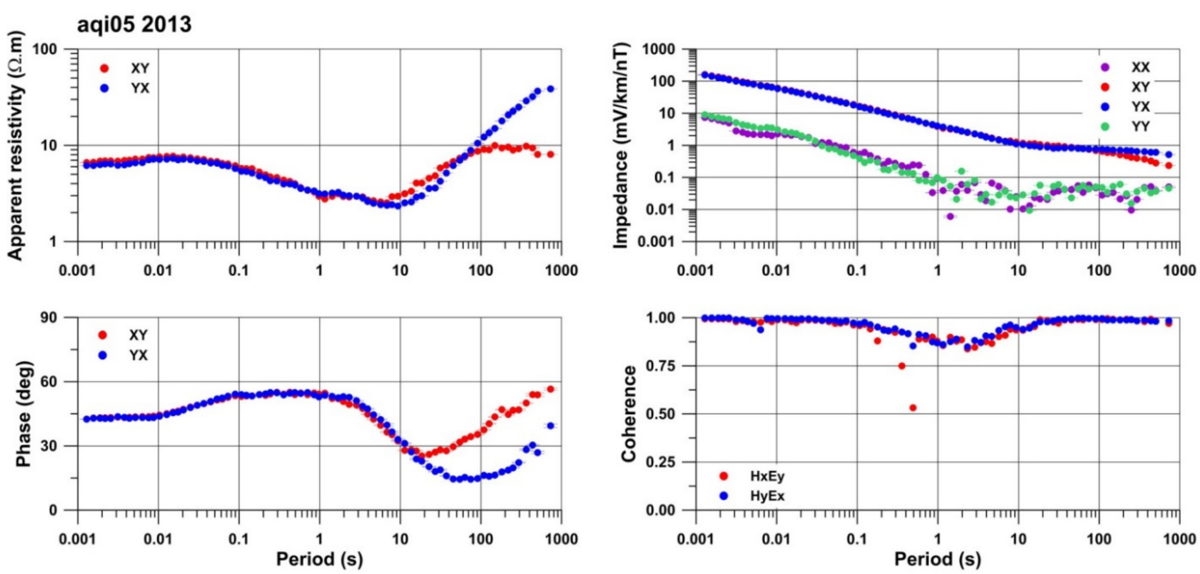

Figure 4. Final AMT-MT responses from site aqi05, 2013 survey, for responses in the geographical coordinate system. The response merges AMT responses obtained using local processing (electric field from aqi05, magnetic field from aqi08) and MT responses also obtained using local processing (electric field from aqi05, magnetic field from aqi02). Left panels show the apparent resistivity and phase response for the north-south (*xy*) and east-west (*yx*) off-diagonal components of the impedance response. The upper right panel shows the four components of the impedance tensor and the lower right panel shows the coherence between orthogonal electric and magnetic field components. Error bars are smaller than the symbol size.

Figure 5 shows a synthesis of the 2013 AMT and MT results from the Aquistore area. The overall response has a similar form at all sites and, except at two anomalous sites, it is almost identical to the aqi05 response shown in Fig. 4. Small differences in the response at different sites occur at very short periods (<0.003 s) and at very long periods (>30 s). In the short period range the apparent resistivities range from 4 to 20 Ωm, while the phases range from 35˚ to 60˚ (Fig. 5). The variations are attributed to spatial variations in the shallow resistivity structure due to lateral changes in surficial sediments and back-fill. The differences between responses at different sites in the long period range are much smaller and are attributed the resistivity structure within the Precambrian crust including the NACP conductor. The results indicate the MT response at the Aquistore site is locally 1-D but spatially variable at short periods, regionally 1-D at intermediate periods, and 2-D at the longest periods.

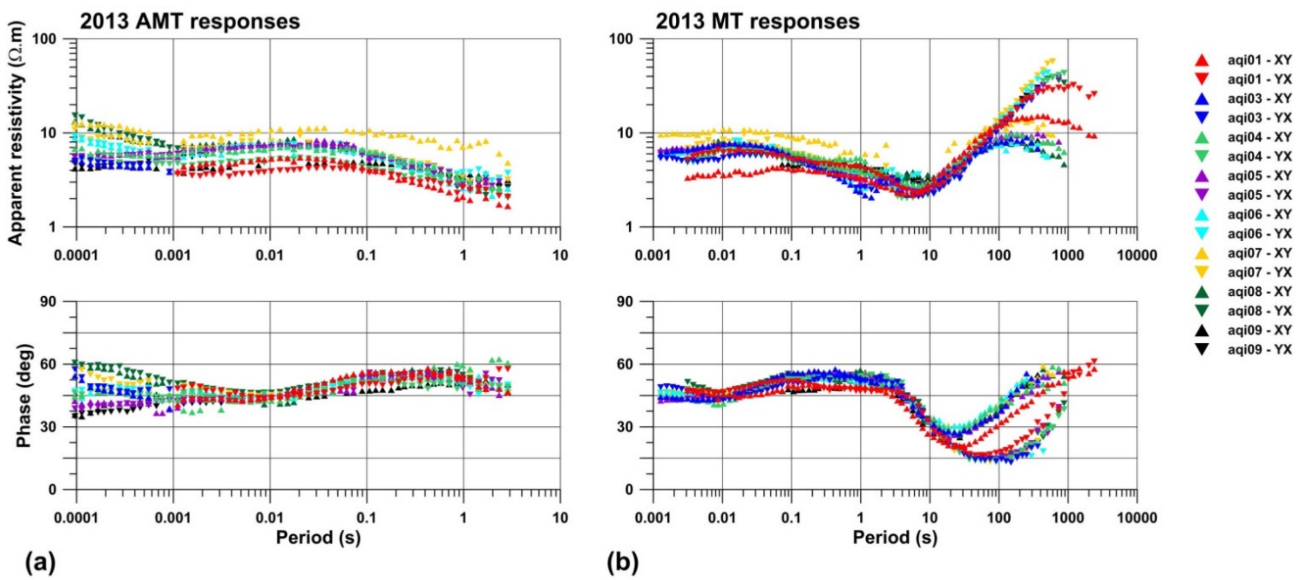

Figure 5. Synthesis of 2013 responses: **(a)** AMT and **(b)** MT. The AMT responses are remote-referenced and the MT responses are locally-processed results. The period ranges are plotted separately to show the overall form of the separate responses from each acquisition type.

Figure 6 shows pseudosection of the MT *xy*- and *yx*-impedance response along a southwest to northeast profile that includes MT responses from two controlled-source electromagnetic sites as well as sites from the main MT survey area. The figure shows the spatial variations in the MT response occurring at short periods and at long periods that are noted in Figure 5. The response at intermediate frequencies is more spatial uniform and similar for the two modes, except at sites near the injection well, indicating a response that is close to one-dimensional.

The responses at different sites were compared statistically using a normalized root mean square (RMS) measure in order to support the interpretation of one-dimensionality. For sites *A* and *B* the total misfit is:

$$E = \sqrt{\frac{1}{2mn}\sum_{i=1}^{n}\sum_{j=1}^{m}\frac{\left|Z_j^A(T_i) - Z_j^B(T_i)\right|^2}{\left|Z_j^A(T_i)\right|\cdot\left|Z_j^B(T_i)\right|}} \qquad \text{Eq. 5}$$

where *n* is the number of periods considered and *m* is the number of impedance elements considered. Examination of the total misfit between different Aquistore MT sites showed that estimates based on all four impedance terms are dominated by the contribution from the smaller, less well-determined diagonal impedance terms. Subsequent comparisons were therefore made in terms of either the two off-diagonal terms or the individual impedance terms. Comparisons using the whole period range of the Aquistore data show the misfit is dominated by contributions from short and long-periods, as seen in Fig. 5. At intermediate periods, the differences between the response at pairs of sites calculated using equation 5 is typically less than 0.01 to 0.03 (1 to 3%) even between sites aqi02 and aqi15 which are located at the extreme ends of the study area (Fig. 1). This result supports the interpretation of a regionally 1-D structure for the period range from ~0.01 s to 10 s. The very small differences between sites and very small differences between the *xy* and *yx* responses (Fig. 5, 6) could be caused very subtle departures from an exact 1-D structure or by azimuthal anisotropy within the sedimentary sequence, but these features are below the resolution of the current MT data. For example, the observed differences may also be explained by minor source-field bias or correlated noise effects in corresponding frequency range of the MT response.

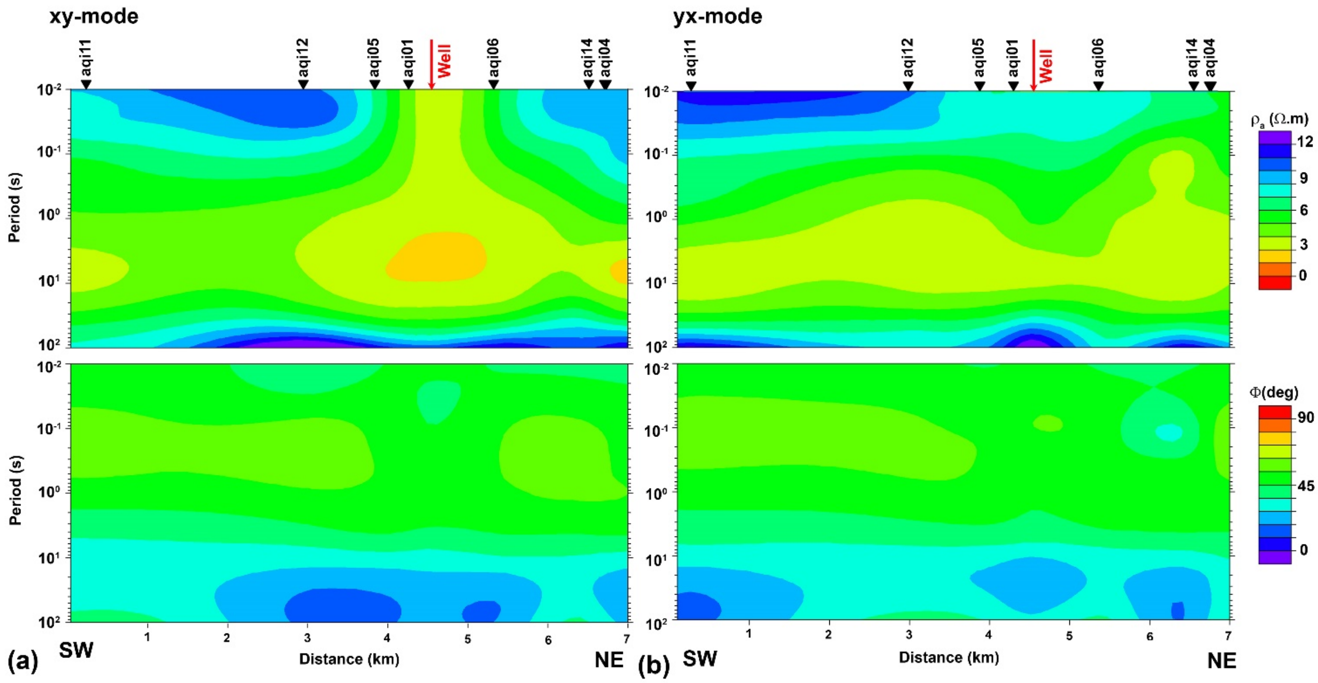

Figure 6. Pseudosections along a southwest-northeast profile through the centre of the study area for (a) the geographic *xy*- impedance component and (b) the geographic *yx*-impedance component. Upper panels show the apparent resistivity response and lower panels show the phase response. The apparent resistivity response is plotted using an unconventional linear colour scaling in order to emphasize lateral changes in the response.

One of the Aquistore MT sites with an anomalous response is aqi01 (Fig. 5, 6). The aqi01 response is a well-defined response differing from that at nearby sites over the whole period range. The response was reproduced in the 2014 and 2015 data sets. At periods longer than 1 s, the anomalous aqi01 response is attributed to galvanic distortion of the regional response. Galvanic distortion of 2-D responses produces a mixing of the impedance modes and this effect is evident in the decreased split between the Z_{xy} and Z_{yx} phase responses at aqi01. An unconstrained fit to the data using the Groom-Bailey distortion model (Groom & Bailey, 1989) yields relatively constant shear values of ~8^{o} and twist values increasing from 0^{o} to 25^{o} over the period range between 10 s and 1000 s. At periods < 10 s the anomalous component of the aqi01 data includes small phase differences from the response at adjacent sites and a strong decrease in the Z_{xy} apparent resistivity. These observations indicate inductive distortion of the aqi01 response. The anomalous site response at aqi01 is attributed to distortion caused by a local conductor. As shown in Fig. 1, the site lies close to both the injection well and the CO_2 pipeline. Results for the Hontomín CO_2 sequestration study site suggest that cased vertical wells cause minimal distortion of the MT response (e.g., Ogaya et al., 2014) so the distortion observed at aqi01 is interpreted to be due to horizontal components of the metallic infrastructure near the injection well.

Site aqi07 also displays different apparent resistivity responses from other 2013 AMT and MT sites and in particular in the *xy* component. The final aqi07 response is noticeably noisier than most other sites, and the anomalous response is attributed to residual effects from the high noise levels. The MT instrumentation was relocated to a new location (aqi13 in Fig. 1) during the 2013 survey, but the level of noise at this site was again very high, precluding calculation of any impedance response. As a result of these issues, aqi07 and aqi13 were not re-occupied in subsequent surveys. Aqi07 and aqi13 lie quite close to the CO_2 pipeline which was under construction during the 2013 MT survey (Fig. 1).

6. CONSTRAINED 1-D INVERSION

Based on the strongly 1-D form of the pre-injection MT responses over the intermediate period range the MT observations were inverted using a 1-D approach. It is noted that for modelling the effects of a CO_2 plume and/or inverting data collected after CO_2 injection it will necessary to use 3-D methods. Also, such an approach will be required to model the effects of the metallic infrastructure such as the injection well and pipelines.

Figure 7a compares the MT response at aqi05 with the response of a forward model based on the well-log data. In order to create a complete resistivity section, the upper 6 Ω.m layer in the simplified well-log model (Fig. 3) was extended to the surface to represent the surficial sediments at depths above the top of the well log at 18 m depth. A uniform half-space of 1000 Ω.m was inserted below the base of the well-log to represent the underlying Precambrian resistivity structure. The MT response of the well-log model response was calculated using the standard 1-D recursion relationship (Wait, 1954). The model response reproduces the aqi05 MT response quite well but there are some significant differences (Fig. 7a). Some of these differences are due to the assumed resistivity of surficial and Precambrian layers. For example, at short periods the observed MT data have a phase of less than 45^{o} suggesting the presence of a thin conductive layer at the surface. In contrast, the well-log model response is based on a thick uniform surface layer so has a phase of 45^{o}. At long periods the 1-D well-log model response is closer to the TM *yx*-responses than the conductive TE *xy*-responses associated with the NACP conductor. There are also some differences in the observed and well-log model responses associated with reduced data quality e.g., in *xy*-component in the AMT dead-band (Viljanen, 2012) at 10^{-3} s (Fig. 7). In addition to these differences, there are significant differences at intermediate periods that indicate differences in the sensing of the resistivity structure by the well-log and MT methods. At periods between 0.01 s and 1 s, the well-log model apparent resistivity response is smaller, or more conductive, than the MT response. The higher phases in well-log response centered on 0.01 s period, and lower phases in the well-log response centered on 1 s period, are also consistent with the well-log model that includes more conductive layers than are sensed by the MT measurement.

In order to obtain a representative conductivity model for the Aquistore site compatible with MT observations, we conducted constrained 1-D inversions of the MT data from aqi05 using the well-log data as a reference model. This approach was taken in order to make use of detailed information on resistivity layering provided by the well-logs while accommodating the differences that may arise in the sensing of the resistivity structure by surface MT measurements. The aqi05 data were chosen as they provided a high quality representation of the almost 1-D MT response of the Williston Basin rocks in the study area. The model was parameterized in terms of the log resistivity with each layer having a fixed thickness. This parameterization reflects the accurate knowledge of layer depths from the well-log information. The data were not weighted by either the calculated errors or an error floor but, in order to balance the contribution of apparent resistivity and phase responses, the data were parameterized in terms of the log apparent resistivity and phase in radians. In addition, the misfit from period ranges corresponding mainly to the response of surficial sediments and Precambrian rocks, as well as from bands of poorer data quality (Fig. 7a) was down-weighted by a factor of 2. The non-random distribution of the misfit that was obtained in the 1-D inversions precluded the use of a statistically-defined target fit. In order to examine the influence of the slight differences in the observed *xy*- and *yx*-responses, separate inversions were done of the higher quality *yx*-data first followed by inversions of the *xy*-data. The *yx*-data are also only minimally affected by the nearby NACP conductor (Jones, 1993).

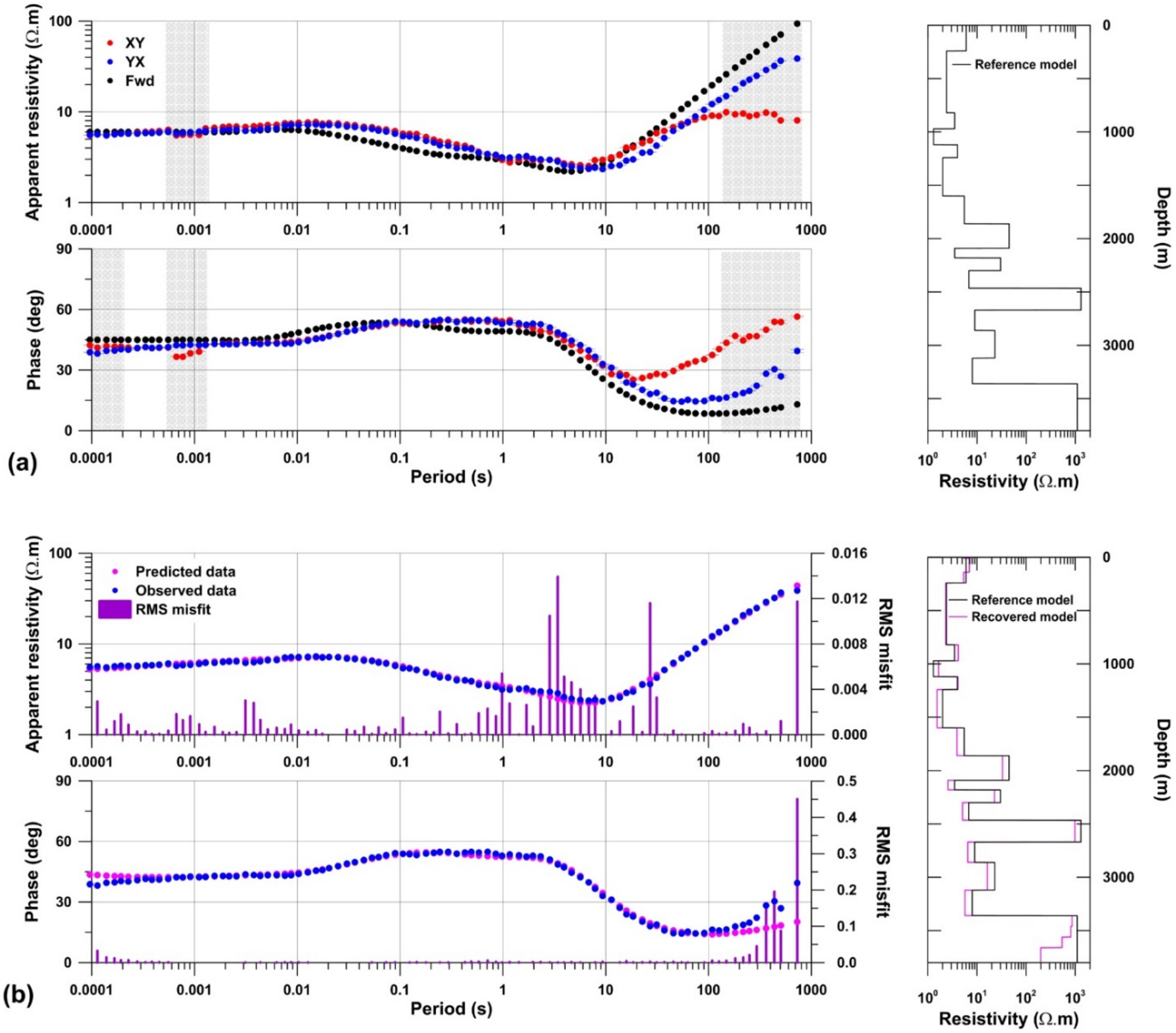

Figure 7. Comparison of observed aqi05 MT responses with theoretical model responses. **(a)** Observed aqi05 responses (*xy*-mode in red and *yx*-mode in blue) and forward response (black) from reference well-log model shown to the right. Shaded bands are down-weighted in the inversions. **(b)** Observed aqi05 *yx* response (blue) and forward response of recovered inversion model (magenta). Crimson bars show the RMS misfit at each period. The panel on the right compares the reference model (black) and the inversion model (magenta).

The constrained 1-D inversion minimized an objective function:

$$\phi = \left\| \mathbf{W_D} \left(\mathbf{d} - \mathbf{A}(\mathbf{m}) \right) \right\|^2 + \alpha \left\| \mathbf{W_M} \left(\mathbf{m} - \mathbf{m_0} \right) \right\|^2 \qquad \text{Eq. 6}$$

where α is the relative weighting between the data misfit and model structure objectives, $\mathbf{d}$ is the vector of observed MT data, $\mathbf{A}(\mathbf{m})$ is the non-linear response of the resistivity model $\mathbf{m}$, $\mathbf{W_D}$ is a data weighting matrix, $\mathbf{m}_0$ is the reference model, and $\mathbf{W}_M$ is a measure of model regularization (e.g. damping or smoothing). A Levenberg-Marquardt algorithm was used to solve the linearized inversion problem (e.g., Aster et al., 2005). The well-log resistivity model was used as both the starting model and reference model $\mathbf{m}_0$ in the inversion. Because this model was expected to be close to the final model, the Jacobian (sensitivity) matrix for the starting model was used through all the inversion steps. A resolution matrix based on this Jacobian matrix was calculated in order to examine the approximate relative resolution of the model parameters.

Several preliminary inversion runs were completed before the final inversion of the *yx* responses. Initial results showed that one-layer parameterization of the near-surface layers and Precambrian rocks was insufficient to allow a good data fit at short (<0.001 s) and long periods (>100 s). Although these geological units were not the focus of the inversions, their resistivity structure has some impact on the response at periods corresponding to the Williston basin rocks. Therefore, additional layers were added at shallow and large depth in the model to allow improved data fits. Testing indicated that model regularization (through the $\mathbf{W}_M$ term) involving equally weighted damping, flattening, and smoothing yielded satisfactory results. Finally, tests indicated that the optimal value of α (for the case of equally weighted damping, flattening, and smoothing) is between 0.1 and 1. This range of values yield a data fit that is close to the minimum value while allowing a maximum contribution from the model regularization. Values of $\alpha<1$ do not decrease the data misfit significantly whereas values >10 produce substantially increased data misfit.

Figure 7b shows the data fit and model obtained in the final inversion of the *yx* response and Table 2 lists the resistivity values of the units. The (non-normalized) RMS data misfit of 0.464 was achieved after 6 iterations. The misfit occurs mainly at short and long periods where it can be attributed to limitations in the representation of the true resistivity structure, the largest misfit arising because of the difficulty in fitting very long-period (>300 s) phase responses. There is also some minor misfit at periods near 10^{-2} s and in the period range from 2 to 30 s. At depths of less than 1240 m (above the Mannville layer) the layers in the model derived from the *yx* MT response are mostly more resistive than the well-log model although the layers corresponding to the Belly River and Bearpaw formations are a little more conductive. At greater depth (beneath the Vanguard-Watrous layer) the MT model layers are consistently more conductive than the well-log model. In this depth range, the resistivity values in MT model are consistently 20-30% lower than the well-log values.

Inversion of the *xy*-responses used the final *yx*-model as the starting model and reference model. In the final inversion run, a model was obtained with an RMS misfit of 1.26 after 100 iterations. The changes in the resistivity of each layer of the *xy*-inversion model relative to the well-log are less consistent than for the *yx*-results but support the earlier results (*xy* results not shown). For all of the conductive layers, the resistivity of the *xy* inversion model is higher than for the *yx* model providing a suggestion of azimuthal anisotropy. However, the MT data set has insufficient resolution to fully resolve this result.

Table 2: Comparison of inversion models with reference model and longitudinal resistivity estimates

Layer	**Thickness (m)**	**Resistivity models (Ω.m)**				**Main geological formations**
		Reference	**Long. Resist.**	***yx***	***xy***	
1	10	6		5.34	5.46	Till
2	50	6	6.18	7.19	7.78	Ravenscrag
3	80	6	6.42	6.97	7.10	Ravenscrag
4	100	6	5.37	5.36	5.91	Bearpaw
5	580	2.4	2.35	2.31	2.44	Belly River
6	150	3.5	3.08	4.17	2.60	Belly River-Colorado
7	150	1.3	1.35	1.66	1.3	Colorado
8	120	4	4.43	4.10	4.12	Mannville
9	360	2	2.07	1.55	1.82	Vanguard, Shaunavon, Gravelbourg, Watrous
10	260	5.5	3.35	3.91	5.75	Charles
11	230	45	32.9	33.0	35.2	Mission Canyon, Lodgepole
12	90	3.5	3.80	2.58	5.49	Bakken, Torquay
13	120	30	11.4	22.8	23.9	Birdbear, Duperow
14	165	6.8	4.12	5.09	6.39	Souris River
15	205	1300	262	986	994	Dawson Bay, Prairie Evaporite
16	190	9	5.01	6.47	9.20	Winnipegosis, Ashern, Interlake
17	260	23	14.3	16.3	18.8	Stonewall, Stony Mountain, Red R.
18	240	8	3.45	5.70	10.0	Winnipeg-Deadwood
19	100	1000		867	8789	Precambrian
20	100	1000		815	1232	Precambrian
21	100	1000		540	1519	Precambrian
Half-space		1000		198	913	Precambrian

Figure 8 shows the resolution matrix for the *yx*-response inversion. The ability to independently resolve a parameter is reflected by the magnitude of the corresponding diagonal element relative to the other elements in the same row or column. The covariance of a model parameter with other model parameters is reflected by the magnitude of the corresponding off-diagonal elements. Elements with larger magnitude also indicate a larger influence of that inversion parameter on the MT response. In general, the model resolution is higher for more conductive layers, thicker layers, and layers closer to the surface. There is quite good resolution of the shallowest layers in the model (parameters 1 to 3) and of the conductive Belly River Formation (parameter 5). At greater depth, there is increased model resolution in layers corresponding to the Colorado Group (parameter 7) and the Jurassic Vanguard to Watrous Formations (parameter 9). However, for deeper conductive layers, the covariance is relatively high between the resistivity of some of the underlying layers. The response is sensitive to the resistivity of the Bakkan-Torquay layer (parameter 12), Souris River layer (parameter 14), Interlake-Winnipegosis layer (parameter 16), and Deadwood-Winnipeg layer (parameter 18) but the spread of enhanced model resolution values around the diagonal for these layers indicates that the MT method is unable to resolve the resistivity of these layers independently. The response is completely insensitive to resistive layers such as the Prairie Evaporite-Dawson Bay layer (parameter 15).

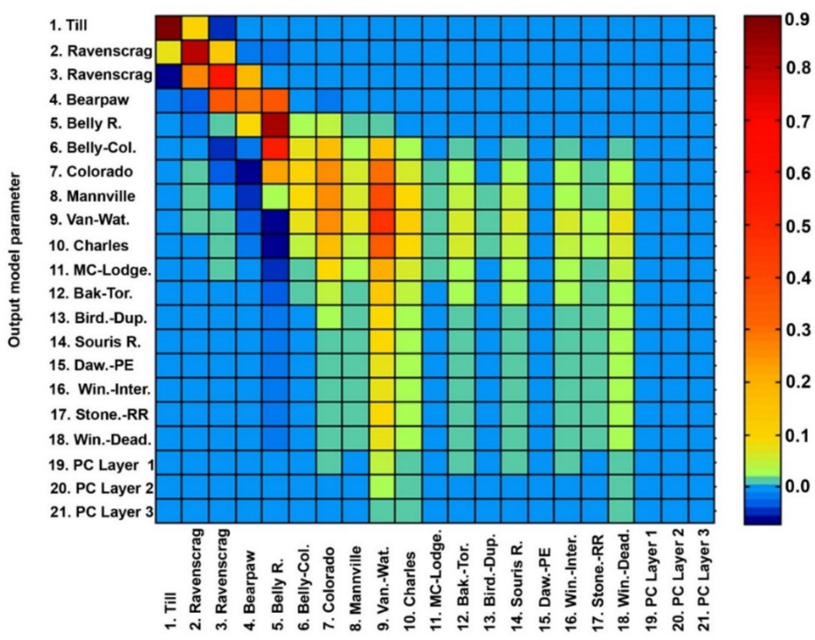

Figure 8. Model resolution matrix for the constrained 1-D inversion of the *yx*-response. The model parameters are the resistivity of each layer defined in Table 2 with the exception of the bottom half-space that has been excluded. The magnitude of the terms indicates the sensitivity of the response to the parameter. The ability to independently resolve a parameter is reflected by the magnitude of the corresponding diagonal element relative to the other elements in the same row or column and the covariance of a model parameter with other model parameters is reflected by the magnitude of the corresponding off-diagonal elements.

The differences between the *yx*-mode inversion model and well-log model can be examined in light of the model resolution. The model resolution results suggest that the increased conductivity of the deeper units (>1240 m) relative to the well-log values is a well-determined result. However, the model covariance indicates the MT method is unable to resolve how the decreased resistivity is distributed between individual layers. The higher conductivity of the layers in the deeper Williston Basin in the inversion model is consistent with the MT method sensing of the longitudinal resistivity of the more strongly stratified units (Fig. 3) present at these depths. Table 2 shows the estimate of the longitudinal resistivity of each layer obtained from the 3 m resampled well-log information. In the more strongly anisotropic Paleozoic units, the inversion model resistivity is generally closer to the longitudinal resistivity estimated from the well-log than the reference model.

7. NOISE CHARACTERIZATION AND MT RESPONSE REPEATIBILITY

Outside the AMT dead-band at 10^{-3} s and the MT dead-band at 1 s (Viljanen, 2012) and period ranges affected by local noise sources, the quality of the Aquistore MT and AMT recorded in the 2013-2015 MT surveys is quite high. Some degradation of the response occurs in the dead-bands; Fig. 8 shows examples of the signal decease in the AMT dead-band that lead to the decreased signal-to-noise ratio in this period band. For recordings made during times of higher signal levels, the response is mostly of high quality in the MT dead-band (McLeod, 2016).

There are a number of forms of electromagnetic noise observed in the Aquistore MT data. The two best characterized sources are 60 Hz powerline harmonics and broadband noise interpreted to be associated with pipeline monitoring or protection systems. The noise was examined and characterized using methods including time-series inspection, spectral analysis, wavelet transform, and polarization determination (McLeod, 2016). More advanced methodologies (e.g., Weckmann et al., 2005; Escalas et al., 2013) may be applied in future studies to characterize more subtle sources.

7.1 Higher harmonics of 60 Hz noise powerline noise

Prior to the MT surveys, the powerline 60 Hz noise was expected to be strong in the vicinity of the Boundary Dam power station. Much of this noise is removed from the MT recordings by the notch filters present in the Phoenix Geophysics MTU instrumentation. However, filtering is not applied to the recordings in the highest AMT frequency band which is sampled at 24,000 Hz. Fourier analyses of the corresponding time series shows clear spectral peaks at up to the ninth odd harmonic (18^{th} actual harmonic) of the 60 Hz signal at 1,140 Hz and the effects may extend to even higher frequencies. This time series is used to define the response at frequencies of >900 Hz and the 60 Hz harmonics lead to some degradation of the MT responses in the AMT dead-band, at times of low signal level. This effect is strongest at aqi04, the site nearest to the power station and its associated infrastructure (Fig. 1).

7.2 Broadband noise from CO_2 pipeline

The 2014 MT recordings at all of the Aquistore sites in the main study area were affected by strong electromagnetic noise. Spectral analyses show the noise occurs in two broad bands centered on 0.009 s (110 Hz) and 0.08 s (12.5 Hz) (Fig. 9). There is increased power in both electric and magnetic fields at periods longer than 0.03 Hz, with localized spectral peaks at 0.059 (17 Hz) and 0.083 s (12 Hz). A second band of increased power extends between 0.007 and 0.012 s with spectral peaks at 0.008 s (130 Hz), 0.009 s (110 Hz) and 0.011 s (95 Hz). The longer and shorter period noise bands are labelled B1 and B2 respectively in Fig. 9. Wavelet transforms show the signal is pulsed: the B2 signal repeats every 0.05 seconds, and the B1 signal repeats every 0.75 seconds. The noise appears to have persisted throughout the whole 2014 MT survey, although there were some days (e.g., November 14, 2014) in which its level was reduced, but it was not observed on either the 2013 or 2015 survey.

The magnitude and polarization of the noise in the magnetic and electric fields varied across the Aquistore study area. In order to parameterize the noise polarization, vector maps of the 0.11 s (9.4 Hz) responses were generated using vector addition of the electric field E_x and E_y power spectral values and the magnetic flux density B_x and B_y power spectral values (Fig. 10). The spatial pattern shown in the electric field polarization map corresponds closely to the trend of the pipeline that transports CO_2 from the power plant to the injection site. The electric field vectors are subparallel to the trend of the nearest segment of pipeline across the survey area and the noise magnitude tends to decrease with distance from the pipeline, for example, there are progressively smaller responses at sites aqi12, aqi11, and aqi10 (Fig. 1). At locations neat straight-line segments of the pipeline, magnetic vectors are approximately perpendicular to the electric field vectors.

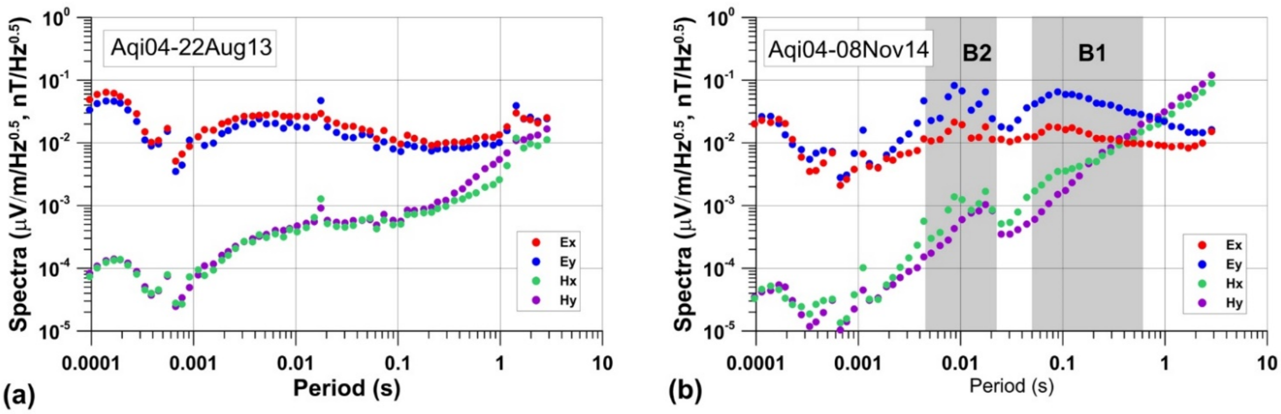

Figure 9. AMT electric field and magnetic flux density power spectra for aqi04 for **(a)** August 22, 2013 and **(b)** November 8, 2014. The shaded rectangles B2 and B1 are the period bands in which the broadband noise caused strong degradation of the 2014 MT responses. Note the decreased signal levels in the AMT dead-band on both data sets. The peak at 2.0 s in the 2013 data set is caused by the controlled-source electromagnetic signal. The magnetic flux density **B** is related to the magnetic field **H** by $\mathbf{B}=\mu_0\mathbf{H}$ where μ_0 is the magnetic permeability of free-space.

The orientation and magnitude of the electric and magnetic vectors supports the interpretation of the noise originating from the CO_2 pipeline. At sites close to individual pipeline segments, the response has the expected form of a line-source (e.g., Junge, 1996). However, departures from this form, including smaller than expected electric field magnitudes near aqi01 and aqi05 and non-orthogonality of electric and magnetic vectors, occur at locations near the ends of the pipeline or equidistant from multiple pipeline segments. These responses can be attributed to the three-dimensional form of the source. The most likely cause of the noise appears to be a pipeline mapping system. These systems rely on the measurement of the fields created by currents injected onto pipelines to detect pipeline location, imperfections in the pipeline or its insulating coating, and other features. The systems often inject both a low frequency (<10 Hz) signal to provide an approximately DC response and a higher frequency signal (~100 Hz) to provide an AC response (Varela et al., 2015). These frequencies lie within the two bands of noise observed in the 2014 MT data. An alternative explanation of the noise is that it is due to an anti-corrosion cathodic protection system (Szarka, 1988; Junge, 1996; Ferguson, 2012). However, this explanation does not account for the noise observed during the 2013 survey (which has different characteristics from the 2014 noise) or provide an obvious reason for the absence of the noise during the 2015 MT survey.

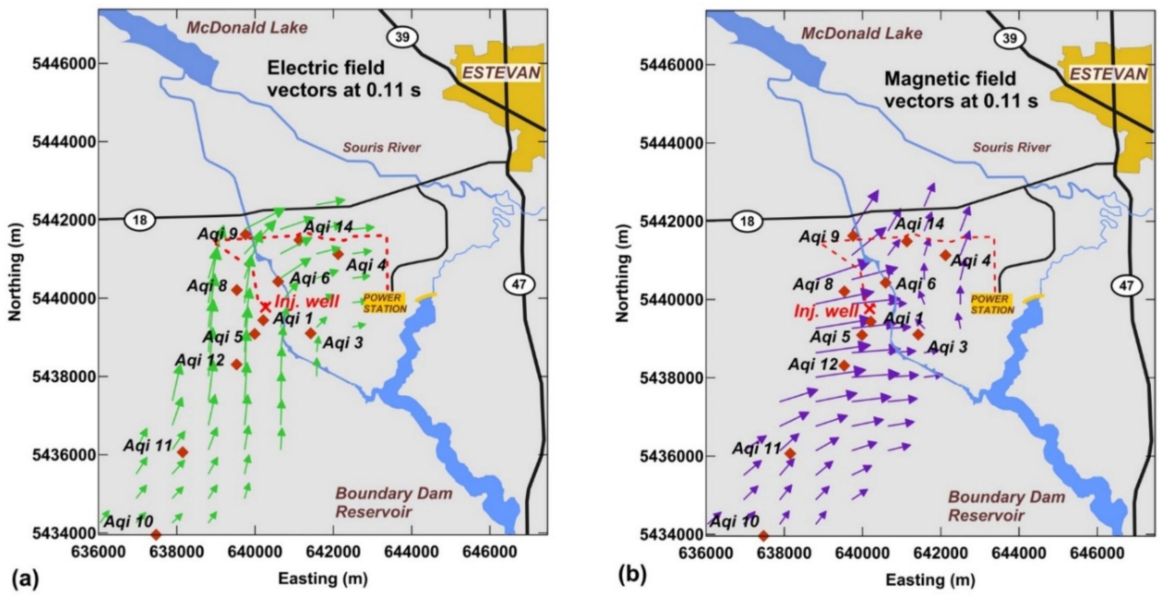

Figure 10. Polarization of noise in the **(a)** electric and **(b)** magnetic field response at 0.11 s (9.4 Hz) in noise band B1. The magnitude and direction of the response was calculated using vector addition of the spectral magnitudes in the power spectra of the *x* and *y*-field components at each MT site. In order to enhance the visibility of the responses, the vector data were gridded using kriging and plotted over an area surrounding the recording sites.

The broad-band noise caused serious degradation of the 2014 MT response requiring complete muting of the MT response in the central period range, typically between 0.1 s and 10 s, but over a broader period range at some sites (aqi01, aqi03, aqi06, aqi08 and aqi14). The muting was based on observation of unrealistic apparent resistivity and phase values derived from the off-diagonal impedance components (Z_{xy} and Z_{yx}). Because the noise at most sites was not aligned in a north-south or east-west direction, it also caused strong effects in the diagonal components of the impedance response (Z_{xx} and Z_{yy}). These effects persisted outside the range of muted data. These effects could be lessened, although not removed, by rotation of the coordinate system to the azimuth of the noise.

Should the broad-band noise be present during future MT surveys at the Aquistore site, it will become necessary to adopt time-, frequency-, and polarization-based approaches for its characterization and removal (e.g., Weckmann et al., 2005; Escalas et al., 2013; Peacock et al. 2013). It may also be possible to use recordings adjacent to the pipeline as a reference noise signal and/or advanced remote-referencing approaches (e.g., Oettinger et al. 2001).

7.3 MT response repeatability

In order to assess the value of the MT method in future resistivity monitoring at the Aquistore site, the repeatability of the MT responses between different surveys was examined. This analysis made use of the 2013 and 2014 MT data sets but for the 2014 data set it was restricted to the period range outside the muted data (McLeod, 2016). Figure 11 shows an example of the comparison of the 2013 and 2014 MT responses. The responses from the different data sets were initially compared using the RMS measure defined in equation 5. As in the comparison of MT responses at different sites, it was determined that the total misfit was dominated by the smaller and less well determined diagonal components. In the temporal comparison, the distortion of the 2014 diagonal responses by the noise caused particularly large errors (Fig. 11). More reasonable misfit estimates were obtained by normalizing the misfit between diagonal terms (e.g., in equation 5) by the corresponding off-diagonal term (assuming that noise was dominant on either the electric field or magnetic field components). Misfits for individual impedance components and periods were also examined and found to be particularly useful. At some sites, the misfit values were observed to rise adjacent to the muted period band and provided a valuable indication of whether the muting was sufficiently extensive.

The results of the repeatability study indicate that within the period range of 10^{-4} to 10^{2} s, but outside the period bands influenced by the broad-band noise occurring in 2014, off-diagonal impedance responses can be measured with a RMS repeatability of 0.01 or 1% or better. This level of repeatability is superior to the level determined by He et al. (2012) for AMT data in a hydraulic fracturing study in southwest China, and to the classification of “quality data sets” established by Peacock et al. (2013) for repeated MT data sets at an enhanced geothermal study site in Australia. The differences are most likely due to the varying ambient noise conditions at the sites. At periods >10^2 s, the misfit increases reflecting the increasing variance in the individual survey results. Eisel & Egbert (2001) also determined higher levels of variance between MT impedance responses at longer period. However, these long period responses would not usually be required in CO_2 monitoring applications.

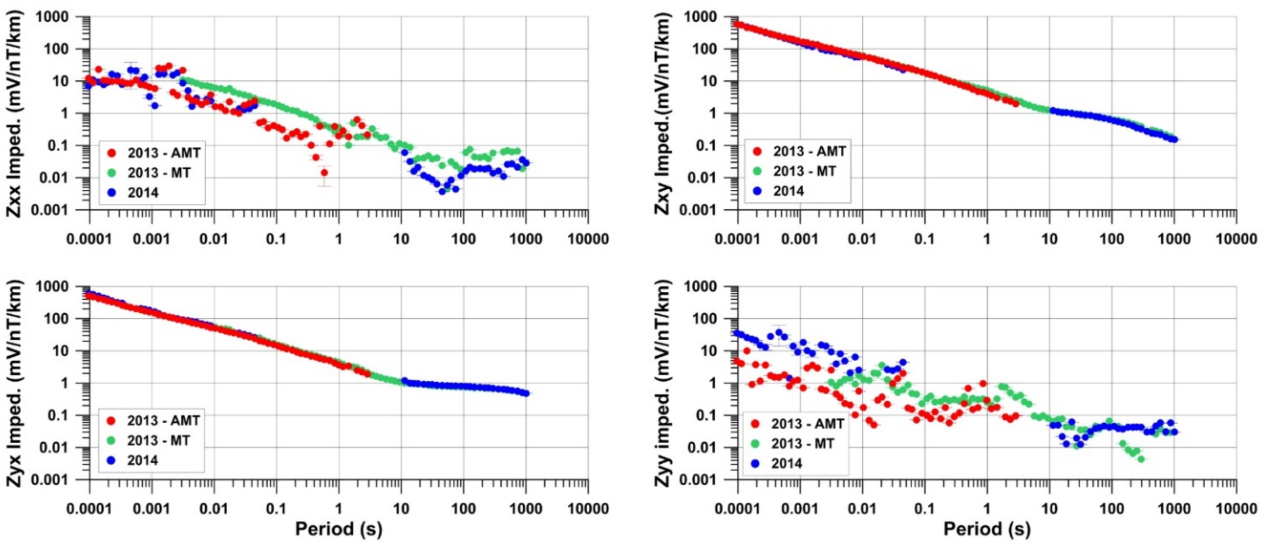

Figure 11. Comparison of MT impedance magnitude at aqi04 from 2013 and 2014 surveys. The 2013 responses are remote reference AMT values and locally-processed MT values and the 2014 responses are the merged AMT and MT responses with noisy period bands muted out.

8. RESOLUTION OF SURFACE ELCTROMAGNETIC METHODS AT AQUISTORE

The Aquistore resistivity structures indicated by the well-log and the constrained MT inversion results were used to compute the theoretical sensitivity of the MT response and controlled-source electromagnetic responses to a hypothetical resistivity changes in the Aquistore reservoir. The MT sensitivity analysis considered only a 1-D model of the reservoir and the controlled-source analysis considered both 1-D and 3-D models.

8.1 1-D MT sensitivity results

The location of the Aquistore reservoir beneath a thick sequence of conductive rocks means that surface MT measurements will have low sensitivity to changes in the reservoir resistivity caused by a CO_2 plume. In order to examine the maximum change in the MT response that would be produced by CO_2 injection, 1-D MT responses were forward calculated for different CO_2 injection scenarios: a pre-injection baseline setting with a relatively conductive 5.7 Ωm reservoir layer between 3120 and 3360 m depth, and two post-injection settings with reservoir resistivities of 20 Ω.m and 50 Ω.m. These values represent a range of CO_2 layer saturations. Based on a simple Archie's Law model for resistivity and a saturation exponent of 2 (e.g., Vilamajó et al., 2013) the resistivity changes correspond to CO_2 saturations of 47% and 67% respectively. Differences between the pre- and post-injection responses occur at periods longer than 1 s (Fig. 12a). The absolute difference in the apparent resistivity response increases to values exceeding ~1 Ω.m at periods > 1 s, but, as the apparent resistivity itself increases in this period range, the proportional change in apparent resistivity is quite small. The phase response provides greater sensitivity to the effects of CO_2 injection and exhibits largest differences between models at a period of 10 s. A maximum phase difference of 1.35° occurs for the 50 Ω.m case. This difference corresponds to an error of 2.4% on the MT impedance estimates and exceeds the estimated 1% repeatability of MT measurements. The result suggests that under ideal circumstances the MT method would be just capable of sensing the effects of a very large CO_2 plume. Also, as discussed below, for more realistic sized plumes of 5 km diameter or less (e.g., Whittaker and Worth, 2011) that cannot be reasonably approximated by a 1-D model, the change in the MT response will likely be below the level of repeatability of routine MT measurements.

Alternative models of the effect of the CO_2 on the pore fluid resistivity will not produce much larger MT responses. In the 1-D MT case, the response is sensitive to conductance of the reservoir layer. Prior to injection the conductance of the 240 m thick 5.7 Ω.m layer is 42.1 S. The 47% CO_2 saturation model causes a decrease in conductance to 12 S and the 67% saturation model causes a decrease to 4.8 S. Higher levels of CO_2 saturation will result in only small additional changes to the MT response. The high salinity of the pore fluids in the Aquistore reservoir means that dissolution of CO_2 is likely to cause only a relatively small increase or decrease in the fluid resistivity and therefore will not yield larger changes in the MT response than the results shown in Fig. 12.

The resolution matrix (Fig. 8) indicates that although the response is sensitive to increased resistivity in the reservoir layer, the results could not be used in isolation to define the depth range of the resistivity change. The change in MT response would be similar for a comparable decrease in conductance in other units in the lower Paleozoic. However, future inversions of time-lapse MT data sets would incorporate strong geological constraints such as limiting the change in resistivity to a fixed depth range by introducing appropriate breaks in the model regularization (e.g., Sarvandani et al., 2017).

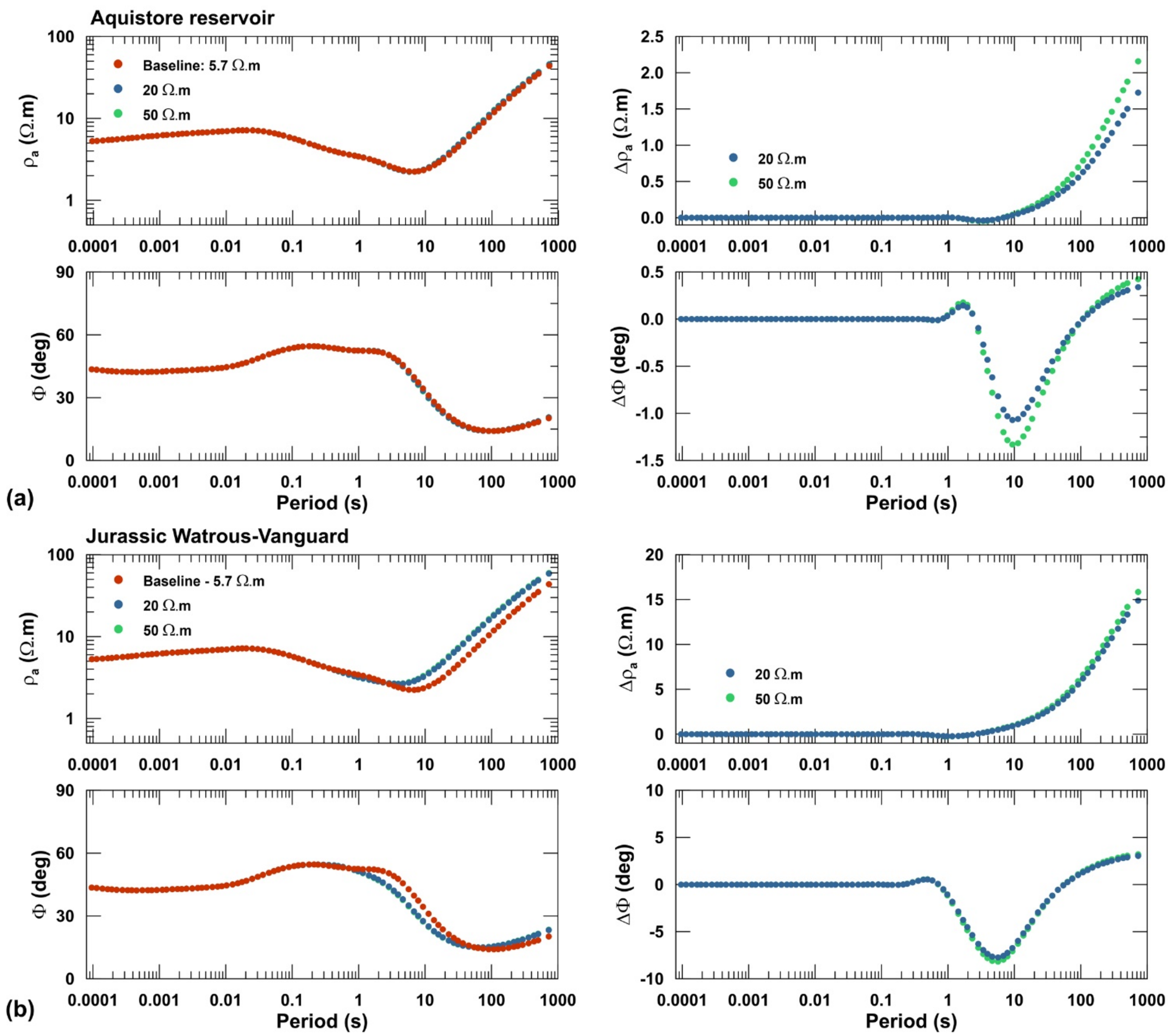

Figure 12. Sensitivity of MT response to changes in layer resistivity. The left panels show the full response and the right panels show the deviation from the baseline response. **(a)** Change in the Winnipeg-Deadwood reservoir between 3120 and 3360 m depth from a baseline value of 5.7 Ω.m to 20 or 50 Ω.m. **(b)** Change in the Jurassic Watrous to Vanguard formations between 1240 and 1600 m depth from a baseline value of 5.7 Ω.m to 20 or 50 Ω.m.

The resolution matrix indicates that for layers in the Williston Basin as deep as the Jurassic Watrous to Vanguard interval (1240-1600 m), there is a higher level of sensitivity (Fig. 8). Figure 12b shows the theoretical changes in the 1-D MT response that would results from the hypothetic situation of CO_2 leakage into this model layer. The anomalies produced in these scenarios are similar in form to those for resistivity changes at reservoir depth, but they occur at a shorter period (10-40 s for apparent resistivity, 5-6 s for the phase) and are larger in magnitude. Differences in the responses from the pre-injection values are apparent in both the apparent resistivity and phase data. The maximum phase anomaly is 8.2˚, corresponding to MT impedance errors of 14.3%. Such changes could be measured more accurately using the MT method. Although, these results are based on 1-D modelling they should also be applicable for resistivity changes over lateral scales of more than several kilometers i.e., plume sizes significantly exceeding the target depth. The MT method therefore has potential for detection of significant CO_2 leakage into intermediate depth strata in the Williston Basin.

The determination of significant changes in the MT phase associated with the modelled changes in the sub-surface resistivity structure, suggests that a purely phase-based response such as the MT phase tensor may be an effective tool for parameterizing the changes in the MT response due to the CO_2 injection, particularly if there is a strong directionality associated with the change in sub-surface resistivity, e.g., at the margins of a CO_2 plume. Peacock et al. (2013) demonstrated the value of the phase tensor response in the MT monitoring of an enhanced geothermal system in Australia.

8.2 1-D controlled-source electromagnetic sensitivity results

Detailed description of the acquisition and analysis of the surface controlled-source electromagnetic measurements at the Aquistore site will be presented in subsequent publications. However, it is valuable to include a brief examination of the sensitivity of these measurements in the present study for comparison with the MT sensitivity results. The surface controlled-source electromagnetic measurements at Aquistore focused on the horizontal electric field response of an electric bipole source. Modelling studies have shown that this configuration can provide good sensitivity for land CO_2 sequestration targets (Streich, 2016; Vilamajó, 2016). A number of authors have described the background theory for such measurements (e.g., Chave & Cox, 1982; Ward & Hohman, 1988; West & Macnae, 1991; Spies & Frischknecht, 1991; Kaufman & Hoekstra 2001; Ingeman-Nielsen & Baumgartner, 2006; Key, 2009). The response for a uniform half-space can be divided into an inductive, or high induction, limit at distance from the source and a resistive, or low induction limit, close to the source. At the transition between the high and low induction regions there is a significant phase anomaly, and for an in-line source and receiver, a doubling of the response magnitude superimposed on the background geometrical decay. Close to the source the electric field response will resemble the DC resistivity response of static electric dipoles. These classifications must be used with care in more complex resistivity environments such as at Aquistore where electromagnetic signal propagation through the resistive Precambrian basement can significantly affect long-offset measurements.

The theoretical sensitivity of controlled-source electromagnetic responses to changes in the underlying 1-D resistivity structure was examined in detail using Fréchet derivatives (e.g., Boerner & West, 1989) to examine the effects of target depth, offset, and frequency in the Aquistore resistivity environment (McLeod, 2016). However, here we present simplified results based on forward modelling of the responses in order to match the MT results (Fig. 12). The calculations were performed using the MATLAB CR1Dmod code (Ingeman-Nielson & Baumgartner, 2006) with the source consisting of a 1 km long bipole and receivers consisting of 50 m electric dipoles located at specified distances form the source. As for the MT sensitivity analysis, the modelling examined the changes from a pre-injection baseline setting with a relatively conductive 5.7 Ωm reservoir layer, and two post-injection settings with reservoir resistivities of 20 Ω.m and 50 Ω.m. The results are presented in terms of the apparent resistivity and phase of the controlled-source electromagnetic response.

At the 3.5 km offset, the controlled-source responses exhibit a transition between high and low induction number between 0.01 and 100 Hz (Fig. 13a). Changes in the apparent resistivity response are observable at frequencies less than ~3 Hz. At low frequencies, these changes are independent of frequency and are the same changes that would be measured using a DC system. Large apparent resistivity changes are noted at intermediate induction number. Phase sensitivity is most significant from 0.02 to 2 Hz with a maximum at 0.5 Hz. At the 3.5

km offset, the maximum changes are small: 0.012-0.017 Ωm for the apparent resistivity and 0.57˚-0.86˚ for the phase. At the longer offsets, the induction number is higher, and there is a slight shift of the maximum sensitivities to lower frequency (Fig. 13b). At a 9.5 km offset the frequency range of maximum change is from 0.2 to 0.6 Hz for the apparent resistivity and 0.3 to 0.4 Hz for the phase. The sensitivities are larger than for the longer offsets; 0.06 Ω.m and 3.4˚ for a 20 Ωm reservoir and 0.08 Ω.m and 4.6˚ for a 50 Ωm reservoir. The impedance errors for the maximum apparent resistivity and phase anomalies are 4.1% and 8.0%, respectively.

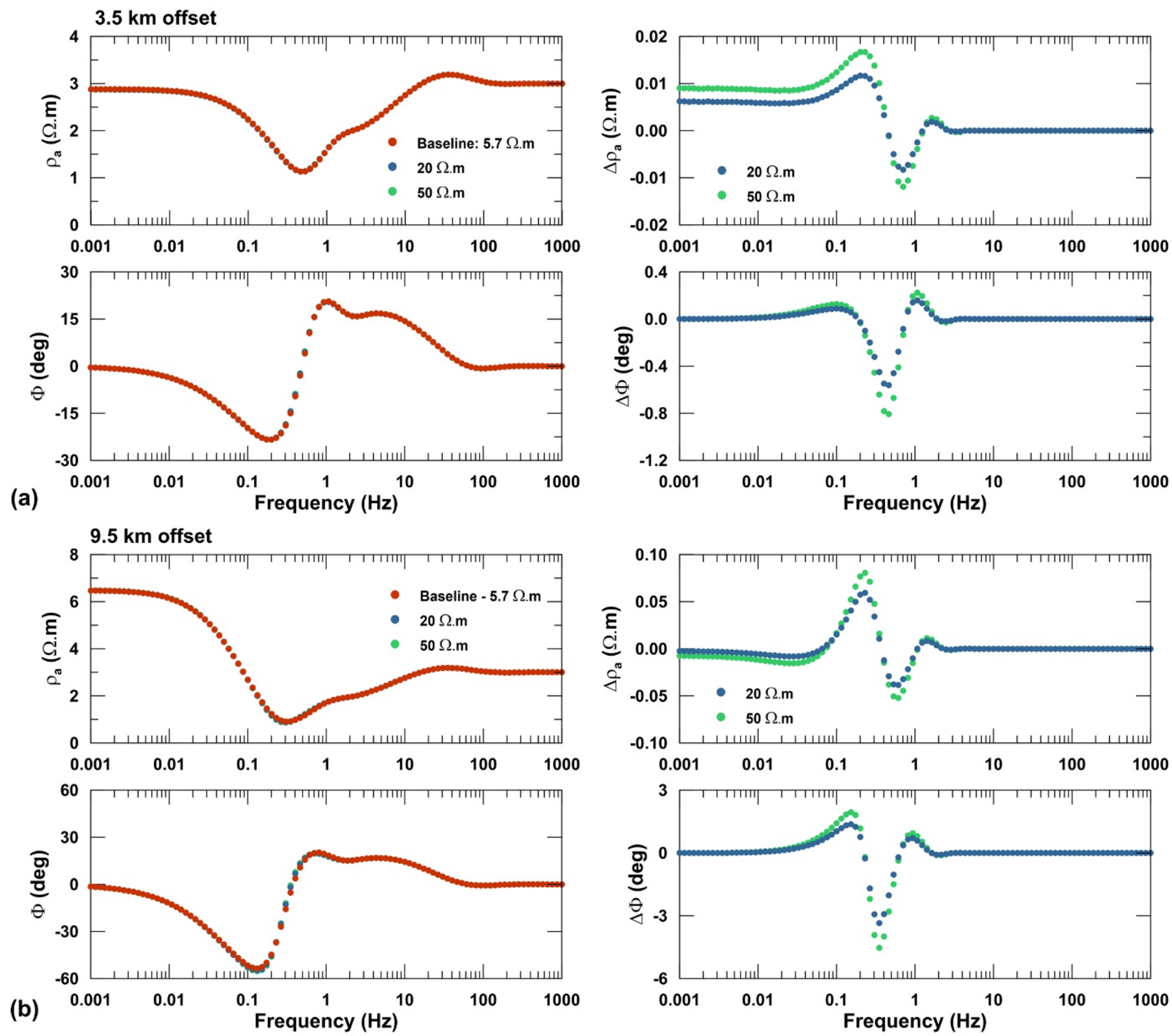

Figure 13. Sensitivity of surface controlled-source electromagnetic response to a change in the resistivity of the Winnipeg-Deadwood reservoir between 3120 and 3360 m depth from a baseline value of 5.7 Ω.m to 20 or 50 Ω.m. The left panels show the full response and the right panels show the deviation from the baseline response. **(a)** Responses at a location 3.5 km from the electric bipole source. **(b)** Responses at a location 9.5 km from the electric bipole source.

The sensitivity of the controlled-source response to changes in the resistivity of the reservoir layer depends on the geometry, frequency and the resistivity structure, and specifically on the offset, frequency, skin-depth in the sedimentary rocks, and skin depth in the Precambrian basement. Maximum phase sensitivity occurs at the transition between low induction number and high induction number type responses. At this frequency there is a contribution to the response from both TE and TM current systems but the changes in the phase response depends most strongly on the TE system. The Fréchet derivative calculations (McLeod, 2016), indicate that the optimal configuration for detecting resistivity changes at the reservoir depth at Aquistore is using longest offset CSEM response at 0.5 Hz.

Compared with the results from the equivalent 1D MT modeling, the optimal CSEM results demonstrate greater sensitivity to the reservoir layer. The minimum required error levels in the MT impedances for detection of the anomalies are 3.5% for apparent resistivity and 2.4% for phase, whereas for the CSEM impedance errors, these thresholds are 4.1% and 8.0%. The maximum MT anomalies occur in the 40-100 s period range compared to 1-5 s for the CSEM anomalies. The increased sensitivity of the CSEM phase response relative to MT phase response is related to the different geometrical configuration of the two sounding methods.

8.3 3-D MT and controlled-source electromagnetic sensitivity results

The 1D MT and controlled-source modeling results in the previous sections are representative of scenarios in which the injected plume is large enough to be approximated as a locally continuous horizontal layer. Three-dimensional calculations were completed to examine the effect of more finite plume dimensions on the response sensitivity. In these calculations, the CO_2 plume is represented by a resistivity change from 5.7 to 50 Ω.m in a rectangular prismatic body at 3120 and 3360 m depth (the same 240 m thickness as the reservoir layer) and variable lateral dimensions. A fully 1D model with a 50 Ω.m reservoir layer was also tested.

For the MT modelling, the response was examined for a period of 10 s, the period of maximum phase change indicated in the one-dimensional modelling (Fig. 12) and at a point on the surface immediately above the centre of the rectangular prism. Examination of the response at other locations shows the maximum MT phase change occurs above the centre of the prism. The modelling used a simplified 7 layer model of the sub-surface resistivity structure in order to match limitations in the corresponding controlled-source electromagnetic calculations. Modelling calculations were done using the three-dimensional finite-difference forward modelling code of Madden & Mackie (1989).

For the CSEM modelling the target was centered at an offset of 3.5 km from the end of the bipole source. The same source and receiver were used as in the 1-D controlled-source electromagnetic analysis and results were obtained for the 0.5 Hz transmission frequency and the 9.5 km offset shown to maximize the sensitivity in the 1-D results (Fig. 13). Modeling calculations were executed in Emigma v8.1 (PetRosEiKon Inc., Orangeville, Canada). This code restricts the number of layers in the model to 8, including the air layer and basal half-space so a slightly simplified resistivity model of the sub-surface was used. The Emigma calculations for the background 1-D responses were verified against the equivalent CRmod1D results.

The results of the 3-D calculations are shown in Fig. 14. For the MT response, as the plume dimensions decrease, the changes in apparent resistivity and phase due to the injection also decrease. Based on the results of Whittaker and Worth (2011), the intermediate sized plumes (5×5 km, 3×3 km, and 2×2 km) are more realistic estimates of the potential Aquistore plume dimensions, and are therefore of greater interest. These plumes generate smaller anomalies, from 20 to 40% of the 1-D phase response, and from 20 to 50% of the 1-D apparent resistivity response.

For the controlled-source electromagnetic results, the effects of large plumes (10×10 km and 20×20 km) are similar to the 1-D change in resistivity due to injection, and demonstrate measurable differences in the phase response. Intermediate sized plumes (5×5 km, 3×3 km, and 2×2 km) generate smaller anomalies, from 6 to 33% of the 1-D phase response, and from 20 to 60% of the 1-D apparent resistivity response. However, the changes in phase response associated with the 3x3 km plumes is still $\sim 1^{o}$. Smaller plumes (1×1 km and 0.5×0.5 km) result in negligible anomalies in the surface controlled-source electromagnetic responses.

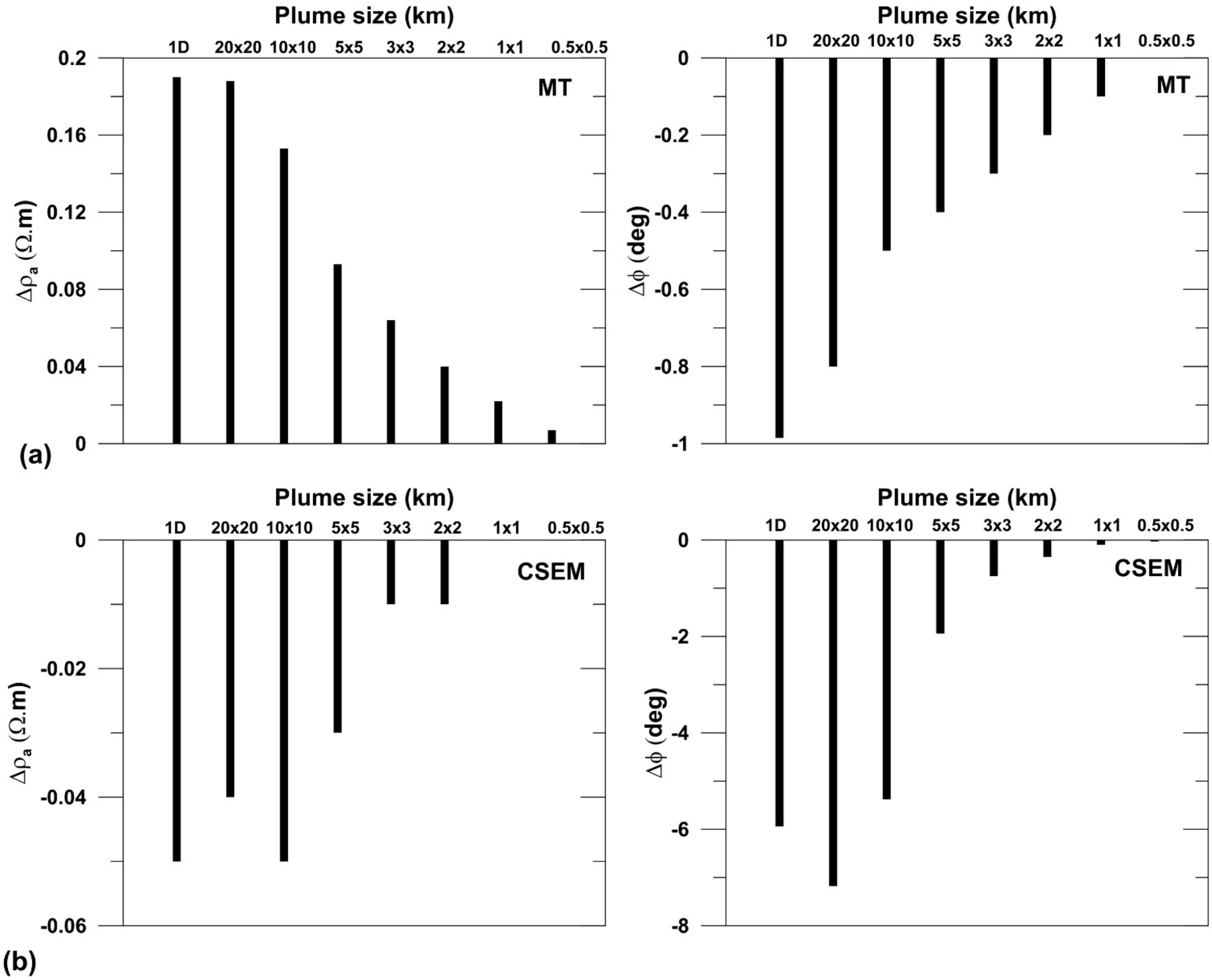

Figure 14. Sensitivity of MT and CSEM responses to a change in the resistivity in Winnipeg-Deadwood reservoir over varying horizontal scales. The results are for a rectangular plume with the dimensions between 20x20 km and 0.5x0.5 km. All results are for a change in resistivity of the Winnipeg-Deadwood reservoir between 3120 and 3360 m depth from a baseline value of 5.7 Ω.m to 50 Ω.m. (a) MT results for a period of 10 s and a site immediately above the centre of the plume. The 1-D results are as shown in Fig. 12. (b) Surface controlled-source electromagnetic response for a site at 9.5 km from the source and with the plume centred on a horizontal position 3.5 km from the source. The 1-D results are as shown in Fig. 13.

The accuracy and repeatability of surface controlled-source measurements at the Aquistore site has not yet been fully established. The exact values will depend on the ambient electromagnetic noise levels at the sites, receiver sensitivity, signal strength at the receiver, duration of the recordings, and ability to replicate the exact survey configuration. However, results from other controlled-source surveys can be used as a general guide to the expected accuracy of the Aquistore responses. For controlled-source surveys at the Hontomín sequestration site in Spain, Vilamajó (2016) determined responses for frequencies of 4 to 32 Hz at most sites had repeatability of better than 1% in the amplitude and 1° in the phase. He reports phase measurement errors of 0.4° to 1.0° using a horizontal electric dipole transmitter. Notwithstanding the differences in the survey configurations and noise levels at the Hontomín and Aquistore sites, the Hontomín repeatability results suggest response repeatability at Aquistore of 1% can be achieved with sufficiently long recording durations. At this level, the changes in surface controlled-source responses due to a plume that can be approximated by a 1-D structure (e.g., $>3^{\circ}$ in the phase response) are expected to be easily measureable and the 3-D modelling results suggest the surface controlled-source method has the capacity to detect the changes in resistivity associated with a moderate-sized (larger than 3x3 km) CO_2 plume. While both the apparent resistivity and phase demonstrate similar types of sensitivity in most scenarios, changes to the phase response are far more likely to be at a detectable level.

9. CONCLUSIONS

This study focuses on the use of MT soundings prior to the commencement of CO_2 injection at the Aquistore CO_2 sequestration site. It examines the data from MT surveys conducted in 2013, 2014 and 2015 over a 4×4 km area surrounding the Aquistore injection well. The objectives of the study are: to characterize the MT response at the Aquistore injection site; to define the background electrical resistivity structure around the Aquistore site; to examine the effects of the noise on surface electromagnetic measurements; and to use the derived resistivity model to conduct preliminary examination of the sensitivity of surface electromagnetic measurements to resistivity changes associated with the injection of CO_2 into the reservoir and leakage into the overlying strata.

The baseline MT surveys successfully defined the MT response at the Aquistore site. The response is locally one-dimensional but spatially variable at short periods (<0.003 s), regionally one-dimensional at intermediate periods (from ~0.01 s to 10 s), and two-dimensional at the longest periods (>30 s). In the short period range the spatial variations are attributed to lateral changes in surficial sediments and back-fill. Strong two-dimensionality observed at long periods (>30 s), along with minor differences between responses at different

Aquistore sites in this range, are attributed to the resistivity structure within the Precambrian crust including the NACP conductor. At intermediate periods, corresponding mainly to the Williston Basin rocks, the MT response is very similar across the Aquistore study area. The RMS response difference between sites is typically less than 1 to 3% even between sites located on either end of the study area. Anomalous responses observed at site aqi001, located several hundred metres away from the injection well, can be attributed to distortion of the MT response by metallic infrastructure.

The observed MT response was inverted using a 1-D approach with constraints from a reference model based on a resistivity well-log. This approach was used in order to make use of the detailed information on resistivity layering available in the well-log while accommodating the different sensing of the resistivity structure by the well-log and MT methods. In order to obtain a good fit to the data over the period range corresponding mostly to the Willison Basin rocks it was also necessary to include appropriate parameterization of near-surface and Precambrian layers. The resulting resistivity model provides a good fit to the observed MT data with the largest misfit arising in fitting the very long-period (>300 s) phase responses. The large-scale features of the resistivity model are similar to those in other models of the Williston Basin. At depths of less than 1240 m (above the Mannville formation) layers in the MT inversion model are mostly more resistive than the well-log model and at greater depth (beneath the Vanguard to Watrous units) the MT model layers are consistently more conductive than the well-log model. In the deeper range, the resistivity values in MT model are consistently 20-30% lower than the well-log values. The higher conductivity of the layers in the MT model is consistent with the MT method sensing of the longitudinal resistivity of the more strongly stratified units present at these depths. The model resolution matrix indicates that the increased conductivity of the deeper units is a well-determined result but that the MT method is unable to resolve how the decreased resistivity is distributed between individual layers.

The electromagnetic noise observed in the Aquistore MT data set included high-frequency odd harmonics of the 60 Hz powerline signal and broad-band noise that was observed only in the 2014 MT data set and which significantly degraded the MT responses determined in that survey. The broad-band noise can be spatially related to the CO_2 pipeline between the power station and the injection well and is interpreted to have caused by a pipeline mapping system. The results of an MT repeatability study indicate that within the period range of 10^{-4} to 10^{2} s, but outside the period bands influenced by the broad-band noise occurring in 2014, off-diagonal MT impedance responses can be measured with a RMS repeatability of 1% or better.

Sensitivity studies based on the Aquistore resistivity model indicate that the MT response at the Aquistore site is minimally sensitive to a CO_2 plume with sufficiently large horizontal dimensions to be approximated by 1-D layer. However, the response of smaller, more realistic, plumes would likely not be detectible by the MT method. In contrast, the MT response would be moderately sensitive to a change in the resistivity in the Jurassic Watrous to Vanguard interval (1240-1600 m), e.g., as caused by hypothetical leakage of CO_2 from the reservoir to shallow depths.

Additional sensitivity studies show that for surface controlled-source electromagnetic measurements using an electric bipole source and electric dipole receivers, at an offset of 9.5 km, the maximum sensitivity to resistivity change in the reservoir will occur in the intermediate induction number response at 0.5 Hz. Phase changes of ~1° or higher, which are expected to be resolved in realistic controlled-source data sets, will occur for plumes larger than about 3x3 km in lateral dimensions. A more extensive evaluation of the sensitivity of controlled-source electromagnetic responses to 1-D and 3-D structures and the results of analysis of the controlled-source electromagnetic measurements completed at Aquistore will be provided in a subsequent paper. These results will also be integrated with the results obtained on the noise sources and resistivity

ACKNOWLEDGMENTS

Aquistore is an independent research and monitoring project managed by the Petroleum Technology Research Centre (PTRC) and the authors gratefully acknowledge the PTRC's Aquistore Project for is support and collaboration on this research.SaskPower facilitated access to the Boundary Dam site. NRCan supported the current research as part of their Integrated CO_2 Measurement, Monitoring and Verification Study. J. McLeod was supported under the Government of Canada Research Affiiate Program. T. Liveda and B. Bancroft assisted in the collection of the 2013 MT data and E. Roots assisted in the collection of the 2014 MT data. A. Frederiksen and P.

Mojabi provided valuable suggestions in their revises of McLedo (2016). We thank the late Dr. A. Hibbs and the GroundMetrics field crew who were instrumental in completion of the 2013 controlled-source electromagnetic survey. A. Bouchedda, (INRS) and J. Silliker (NRCan) provided important assistance in the 2015 controlled-source electromagnetic survey. Comments from two anonymous reviewers led to important improvements in this work.

REFERENCES

Abdelfettah, Y., Sailhac, P., Larnier, H., Matthey, P.D., Schill, E., 2018. Continuous and time-lapse magnetotelluric monitoring of low volume injection at Rittershoffen geothermal project, northern Alsace–France. Geothermics, 71, 1-11. https://doi.org/10.1016/j.geothermics.2017.08.004

Ansdell, K.M. 2005. Tectonic evolution of the Manitoba–Saskatchewan segment of the Paleoproterozoic Trans-Hudson Orogen, Canada. Canadian Journal of Earth Sciences 42, 741-759, http://doi.org/10.1139/e05-035.

Aster, R.C., Borchers, B., Thurber, C.H., 2005. Parameter estimation and inverse problems. Elsevier Academic Press, Burlington, MA, 301 p., ISBN: 978-0128100929.

Auld, D.R., Dosso, S.E., Oldenburg, D.W., Law, L.K., 1992. Monitoring temporal change in conductivity in the central Vancouver Island region, an area with past large earthquakes. Canadian Journal of Earth Sciences, 29, 601-608. https://doi.org/10.1139/e92-052

Bachu, S. 2002. Suitability of the subsurface in Saskatchewan and Manitoba for geological sequestration of anthropogenic carbon dioxide; Alberta Geological Survey, Alberta Energy and Utilities Board, 81 pp.

Bergmann, P., Ivandic, M. Norden, B., Rücker, C., Kiessling, D.,Lüth, S., Schmidt-Hattenberger, C., Juhlin, C., 2014. Combination of seismic reflection and constrained resistivity inversion with an application to 4D imaging of the CO_2 storage site, Ketzin, Germany. Geophysics 79, B37–B50, http://dx.doi.org/10.1190/GEO2013-0131.1.

Bergmann, P., Schmidt-Hattenberger, C., Kiessling, D., Rücker, C., Labitzke, T., Henninges, J., Baumann, G., Schütt, H., 2012, Surface-downhole electrical resistivity tomography applied to monitoring of the CO_2 storage Ketzin (Germany). Geophysics 77, B253– B267, http://dx.doi.org/10.1190/geo2011-0515.1.

Bhuyian, A.H., Landro, M., Johansen, S.E., 2012, 3D CSEM modeling and time-lapse sensitivity analysis for subsurface CO2 storage: Geophysics 77, E343–E355, http://dx.doi.org/10.1190/geo2011-0452.1.

Boerner, D.E., West, G.F. 1989. A spatial and spectral analysis of the electromagnetic sensitivity in a layered earth. Geophysical Journal International 98, 11-21. http://dx.doi.org/10.1111/j.1365-246X.1989.tb05510.x.

Börner, J.H., Herdegen, V., Repke, J-U., Spitzer, K., 2013. The impact of CO_2 on the electrical properties of water bearing porous media – laboratory experiments with respect to carbon capture and storage. Geophysical Prospecting 61, 446-460, http://dx.doi.org/10.1111/j.1365-2478.2012.01129.x.

Börner, J.H., Herdegen, V., Repke, J-U., Spitzer, K., 2015. The electrical conductivity of CO_2-bearing pore waters at elevated pressure and temperature: a laboratory study and its implications in CO_2 storage monitoring and leakage detection. Geophysical Journal International 203, 1072-1084. http://dx.doi.org /10.1093/gji/ggv331.

Bosch, D., Ledo, J., Queralt, P., Bellmunt, F., Luquot, L., Gouze, P., 2016. Core-scale electrical resistivity tomography (ERT) monitoring of CO_2-brine mixture in Fontainebleau sandstone. Journal of Applied Geophysics 130, 23-36, https://doi.org/10.1016/j.jappgeo.2016.03.039.

Bouchedda, A., Giroux, B., 2015. Synthetic study of CO_2 monitoring using time-lapse down-hole magnetometric resistivity at Field Research Station, Alberta, Canada. In *SEG Technical Program Expanded Abstracts 2015* (p. 5529-5533). Society of Exploration Geophysicists, https://doi.org/10.1190/segam2015-5884919.1.

Chave, A.D., Cox, C.S., 1982. Controlled electromagnetic sources for measuring electrical conductivity beneath the oceans. 1. Forward problem and model study. Journal of Geophysical Research 87, 5327-5338, https://doi.org/10.1029/JB087iB07p05327.

Chave, A.D., Jones, A.G., 2012. The Magnetotelluric Method: Theory and Practice. Cambridge University Press, Cambridge (UK), ISBN 978-0521819275.

Chiang C.W., Unsworth, M.J., Chen, C.S., Chen, C.C., Lin, T.S., Shu, H.L., 2008. Fault zone resistivity structure and monitoring at the Taiwan Chelungpu Drilling Project (TCDP). Terrestrial Atmospheric and Ocean Sciences, 19, 473-479. https://doi.org/10.3319/TAO.2008.19.5.473(T).

Commer, M., Doetsch, J., Dafflon, B., Wu, Y., Daley, T. M., Hubbard, S.S., 2016. Time-lapse 3-D electrical resistance tomography inversion for crosswell monitoring of dissolved and supercritical CO_2 flow at two field sites: Escatawpa and Cranfield, Mississippi, USA. International Journal of Greenhouse Gas Control 49, 297-311, https://doi.org/10.1016/j.ijggc.2016.03.020.

Commer, M., Kowalsky, M. B., Doetsch, J., Newman, G. A., Finsterle, S., 2014. MPiTOUGH2: A parallel parameter estimation framework for hydrological and hydrogeophysical applications. Computers & Geosciences 65, 127-135, https://doi.org/10.1016/j.cageo.2013.06.011.

Daley, T.M., Smith, J.T., Breyer, J.H., LaBrecque, D., 2014. Borehole EM monitoring at Aquistore: Final report to the carbon capture project (CCP), 30p.

Dixon, J. 2008. Stratigraphy and facies of Cambrian to Lower Ordovician strata in Saskatchewan. Bulletin of Canadian Petroleum Geology, 56, 93-117.

Edwards, R.N., Wolfgram, P.A., Judge, A.S., 1988. The ICE-MOSES Experiment: mapping permafrost zones electrically beneath the Beaufort Sea. Marine Geophysical Researches 9, 265-290. https://doi.org/10.1007/BF00309977

Escalas, M., Queralt, P., Ledo, J., Marcuello, A., 2013. Polarisation analysis of magnetotelluric time series using a wavelet-based scheme: a method for detection and characterisation of cultural noise sources. Physics of the Earth and Planetary Interiors 218, 31–50, http://dx.doi.org/10.1016/j.pepi.2013.02.006.

Eisel M., Egbert, G.D., 2001. On the stability of magnetotelluric transfer function estimates and the reliability of their estimates. Geophysical Journal International 144, 65-82. https://doi.org/10.1046/j.1365-246x.2001.00292.x

Eliasson, P., Romdhane, A., Jordan, M., Querendez, E., 2014. A synthetic Sleipner study of CO_2 quantification using controlled source electro-magnetics and full waveform inversion. Energy Procedia 63, 4249-4263, https://doi.org/10.1016/j.egypro.2014.11.460.

Ferguson, A.G., Betcher, R.N., Grasby, S.E. 2007. Hydrogeology of the Winnipeg Formation in Manitoba, Canada; Hydrogeology Journal 15, 573-587, https://doi.org/10.1007/s10040-006-0130-4.

Ferguson, I.J., 2012. Instrumentation and Field Procedure. In: Chave, A.D., Jones, A.G. (Eds.), The Magnetotelluric Method: Theory and Practice. Cambridge University Press, Cambridge (UK), ISBN 978-0521819275.

Fowler, C.M.R., Nisbet, E.G, 1984. The subsidence of the Williston Basin. Canadian Journal of Earth Sciences 22, 408-415.

Gamble, T.D, Goubeau, W.M., Clarke, J., 1979. Magnetotellurics with a remote reference, Geophysics 44, 53–68, https://doi.org/10.1190/1.1440923.

Gasperikova, E., Hoversten, G.M., 2006. A feasibility study of nonseismic geophysical methods for monitoring geologic CO_2 sequestration. The Leading Edge 25, 1282–1288, https://doi.org/10.1190/1.2360621.

Gowan, E.J., Ferguson, I.J., Jones, A.G., Craven, J.A., 2009. Geoelectric structure of the northeastern Williston basin and underlying Precambrian lithosphere. Canadian Journal of Earth Sciences 46, 441-464, https://doi.org/10.1139/E09-028.

Grayver, A.V., Streich, R. Ritter, O., 2013. Three-dimensional parallel distributed inversion of CSEM data using a direct forward solver. Geophysical Journal International 193, 1432-1446, https://doi.org/10.1093/gji/ggt055

Groom R.W., Bailey, R.C., 1989. Decomposition of magnetotelluric impedance tensors in the presence of local three-dimensional galvanic distortion. Journal of Geophysical Research, 94, 1913-1925, https://doi.org/10.1029/JB094iB02p01913.

Hanekop, O., Simpson, F., 2006. Error propagation in electromagnetic transfer functions: what role for the magnetotelluric method in detecting earthquake precursors? Geophysical Journal International, 165 763-774. https://doi.org/10.1111/j.1365-246X.2006.02948.x

He, L., Hu, X., Xu, L., He, Z., Li, W., 2012. Feasibility of monitoring hydraulic fracturing using time-lapse audio-magnetotellurics. Geophysics 77, WB119-WB126. https://doi.org/10.1190/geo2011-0378.1

Hibbs, A., 2013, Test of a new BSEM configuration at Aquistore, and its application to mapping injected CO_2, June 26, 2013. BP project Task 1 report, 7 p.

Hovorka, S.D., Meckel, T.A., Trevino, R.H., Lu, J., Nicot, J.-P., Choi, J.-W., Freeman, D.,Cook, P., Daley, T.M., Ajo-Franklin, J.B., Freifeld, B.M., Doughty, C., Carrigan, C.R., Brecque, D.L., Kharaka, Y.K., Thordsen, J.J., Phelps, T.J., Yang, C., Romanak, K.D., Zhang, T., Holt, R.M., Lindler, J.S., Butsch, R.J., 2011. Monitoring a large volume CO_2 injection: Year two results from SECARB project at Denbury's Cranfield, Mississippi, USA. Energy Procedia 4, 3478–3485. https://doi.org doi:10.1016/j.egypro.2011.02.274

Ingeman-Nielsen, T., Baumgartner, F., 2006. CR1Dmod: A MATLAB program to model 1D complex resistivity effects in electrical and electromagnetic surveys. Computers & Geosciences 32, 1411-1419, https://doi.org/10.1016/j.cageo.2006.01.001.

Irvine, J.A. 1978. Estevan map-area. In: Coal resources of southern Saskatchewan: A model for evaluation methodology, Whitaker, S.H., Irvine, J.A. and Broughton, P.L. (eds.); *Geological Survey of Canada Economic*, report 30, *Saskatchewan Department of Mineral Resources*, report 209, *Saskatchewan Research Council* report 20, 49-67.

Jones, A.G., 1988. Static shift of magnetotelluric data and its removal in a sedimentary basin environment. Geophysics 53, 967-978, https://doi.org/10.1190/1.1442533.

Jones, A.G., 1993. The COPROD2 dataset: Tectonic setting, recorded MT data, and comparison of models. Journal of Geomagnetism and Geoelectricity, 45, 933-955, http://doi.org/10.5636/jgg.45.933.

Jones, A.G., Craven, J.A., 1990. The North American Central Plains conductivity anomaly and its correlation with gravity, magnetic, seismic, and heat flow data in Saskatchewan, Canada. Physics of the Earth and Planetary Interiors, 60, 169-194, https://doi.org/10.1016/0031-9201(90)90260-5.

Jones, A.G., Craven, J.A., McNeice, G.W., Ferguson, I.J., Boyce, T.T., Farquharson C., Ellis, R., 1993. North American Central Plains conductivity anomaly within the Trans Hudson orogen in northern Saskatchewan, Canada. Geology 21, 1027-1030, http://doi.org/10.1130/0091-7613(1993)021<1027:NACPCA>2.3.CO;2.

Jones, A.G., Ledo, J., Ferguson, I.J., 2005. Electromagnetic images of the Trans-Hudson orogen: The North American Central Plains (NACP) anomaly revealed. Canadian Journal of Earth Sciences 42, 457-478, https://doi.org/10.1139/e05-018.

Jones, A.G., Katsube, T.J., Schwann, P., 1997. The longest conductivity anomaly in the world explained: sulphides in fold hinges causing very high electrical anisotropy. Journal of Geomagnetism and Geoelectricity 49, 1619-1629, http://doi.org/10.5636/jgg.49.1619.

Jones, A.G., Savage, P.J., 1986. North American Central Plains conductivity anomaly goes east. Geophysical Research Letters 13, 685-688, https://doi.org/10.1029/GL013i007p00685.

Junge, A., 1996. Characterization of and correction for cultural noise. Surveys in Geophysics 17, 361-391.

Kaufman, A.A., Hoekstra, P., 2001. Electromagnetic soundings. Elsevier Science Publishing Company, Amsterdam, 534 p. ISBN: 978-0444500946.

Key, K., 2009. 1D inversion of multicomponent, multifrequency marine CSEM data: Methodology and synthetic studies for resolving thin resistive layers. Geophysics, 74, F9-F20, https://doi.org/10.1190/1.3058434.

Kirkby, A., Heinson, G., Krieger, L., 2016. Relating permeability and electrical resistivity in fractures using random resistor network models. Journal of Geophysical Research: Solid Earth 121, 1546-1564, https://doi.org/ 10.1002/2015JB012541.

Klappstein, G., Rostron, B., 2014. Shallow hydrogeological and hydrochemical characterization of the Aquistore CO_2 sequestration site in Estevan, Saskatchewan, Canada. Energy Procedia 63, 4971-4976, https://doi.org/10.1016/j.egypro.2014.11.526.

Ladanivskyy, B., Zlotnicki, J., Reniva, P., Alanis, P., 2017. Electromagnetic signals on active volcanoes: Analysis of electrical resistivity and transfer functions at Taal volcano (Philippines) related to the 2010 seismovolcanic crisis. Journal of Applied Geophysics. https://doi.org/10.1016/j.jappgeo.2017.01.033

LeFever, R.D., Thompson, S.C., Anderson, D.B., 1987. Earliest Paleozoic history of the Williston Basin in North Dakota. In: Carlson, C.G., Christopher, J.E. (Eds.), Proceedings of the Fifth International Williston Basin

Symposium. Spec. Publ., 9. Saskatchewan Geological Society, Regina, SK, Canada, pp. 22– 36.

McLeod, J., 2016. Electromagnetic monitoring of CO_2 sequestration at the Aquistore site, Estevan, Saskatchewan, Canada. M.Sc. Thesis, University of Manitoba, Winnipeg, Canada.

Madden, T.M., Mackie, R.L., 1989. Three-dimensional magnetotelluric modelling and inversion. Proceedings of the IEEE, 77, 318-333.

Maidens, J.M., Paulson, K.V., 1988. A magnetotelluric investigation under the Williston Basin of southeastern Saskatchewan. Canadian Journal of Earth Sciences, 25, 60-67, https://doi.org/10.1139/e88-006.

Maillet, R., 1947. The fundamental equations of electrical prospecting. Geophysics 12, 529-556, https://doi.org/10.1190/1.1437342.

Oettinger, G., Haak, V., Larsen, J.C., 2001. Noise reduction in magnetotelluric time-series with a new signal–noise separation method and its application to a field experiment in the Saxonian Granulite Massif. Geophysical Journal International 146, 659-669. https://doi.org/10.1046/j.1365-246X.2001.00473.x

Ogaya, X., Ledo, J., Queralt, P., Marcuello, A., Quinta, A., 2013. First geoelectric image of the subsurface of the Hontomín site (Spain) for CO2 geological storage: A magnetotelluric 2D characterization. International Journal of Greenhouse Gas Control 13, 168-179, https://doi.org/10.1016/j.ijggc.2012.12.023.

Ogaya X., Queralt P., Ledo J., Marcuello A. Jones A.G. 2014. Geoelectrical baseline model of the subsurface of the Hontomín site (Spain) for CO_2 geological storage in a deep saline aquifer: A 3D magnetotelluric characterisation. International Journal of Greenhouse Gas Control 27, 120–138, https://doi.org/10.1016/j.ijggc.2014.04.030.

Ogaya, X., Alcalde, J., Marzán, I., Ledo, J., Queralt, P., Marcuello, A. Benjumea, B. 2016. Joint interpretation of magnetotelluric, seismic, and well-log data in Hontomín (Spain). Solid Earth 7, 943-958, https://doi.org/10.5194/se-7-943-2016.

Osadetz, K.G., Kohn, B.P., Feinstein, S., O'Sullivan, P.B., 2002. Thermal history of Canadian Williston Basin from apatite fission-track thermochronology – implications for petroleum systems and geodynamic history. Tectonophysics 349, 221-249, https://doi.org/10.1016/S0040-1951(02)00055-0.

Peacock, J. R., Thiel, S., Heinson, G. S., Reid, P. 2013. Time-lapse magnetotelluric monitoring of an enhanced geothermal system. Geophysics, 78, B121-B130, https://doi.org/10.1190/geo2012-0275.1

Rankin, D., Kao, D., 1978. The delineation of the Superior Churchill transition zone in the Canadian Shield. Canadian Society of Exploration Geophysics Journal, 14, 50-54.

Rees, N., Heinson, G., Krieger, L., 2016. Magnetotelluric monitoring of coal seam gas depressurization. Geophysics 81, E423-E432. https://doi.org/10.1190/geo2016-0072.1

Rickets, B.D., 1989. Western Canada Sedimentary Basin: A Case Study. Special Publication, Volume 30, Canadian Society of Petroleum Geologists, Calgary 320 p.

Roach, L.A., White, D.J., Roberts, B., 2015. Assessment of 4D seismic repeatability and CO2 detection limits using a sparse permanent land array at the Aquistore CO2 storage site. Geophysics 80, WA1-WA13. https://doi.org/10.1190/GEO2014-0201.1

Rosas-Carbajal, M., Linde, N., Peacock, J., Zyserman, F.I., Kalscheuer, T., Thiel, S., 2015. Probabilistic 3-D time-lapse inversion of magnetotelluric data: application to an enhanced geothermal system. Geophysical Journal International 203, 1946–1960. https://doi.org/10.1093/gji/ggv406

Rostron, B., White, D., Hawkes, C., Chalaturnyk, R., 2014. Characterization of the Aquistore CO_2 project storage site, Saskatchewan, Canada. Energy Procedia 63, 2977-2984, http://dx.doi.org/10.1016/j.egypro.2014.11.320.

Sarvandani, M.M., Kalateh, A.N., Unsworth, M., Majidi, A., 2017. Interpretation of magnetotelluric data from the Gachsaran oil field using sharp boundary inversion. Journal of Petroleum Science and Engineering 149, 25-39. https://doi.org/10.1016/j.petrol.2016.10.019

Smith, M., Bend, S., 2004. Geochemical analysis and familial association of Red River and Winnipeg reservoired oils of the Williston Basin, Canada. Organic Geochemistry 35, 443-452, https://doi.org/10.1016/j.orggeochem.2004.01.008.

Spies, B.R., Frischknect, F.C., 1991. Electromagnetic Sounding; In Nabighian, M.N. (Ed.) Electromagnetic Methods in Applied Geophysics, Volume 2, Applications, Society of Exploration Geophysicists, Tulsa, p. 285-425.

Streich, R., 2016. Controlled-source electromagnetic approaches for hydrocarbon exploration and monitoring on land. Surveys in Geophysics 37, 47-80, https://doi.org/10.1007/s10712-015-9336-0.

Streich, R., Becken, M., Ritter, O., 2010. Imaging of CO_2 storage sites, geothermal reservoirs, and gas shales using controlled source magnetotellurics: modeling studies. Chemie der Erde 70, 63-75. http://dx.doi.org/10.1016/j.chemer.2010.05.004.

Streich, R., Becken, M., Matzander, U., Ritter, O. 2011. Strategies for land-based controlled-source electromagnetic surveying in high-noise regions. The Leading Edge, 30, 1174-1181. https://doi.org/10.1190/1.3657078.

Streich, R., Becken, M., Ritter, O. 2013. Robust processing of noisy land-based controlled-source electromagnetic data. Geophysics 78, E237-E247, https://doi.org/10.1190/geo2013-0026.1

Szarka, L., 1988. Geophysical aspects of man-made electromagnetic noise in the Earth – a review. Surveys in Geophysics 9, 287-318.

Thiel, S., 2017. Electromagnetic monitoring of hydraulic fracturing: Relationship to permeability, deismicity, and stress. Surveys in Geophysics 38, 1133-1169. https://doi.org/10.1007/s10712-017-9426-2

Varela, F., Tan, M.Y., Forsyth, M., 2015. An overview of major methods for inspecting and monitoring external corrosion of on-shore transportation pipelines. Corrosion Engineering Science and Technology 50, 226-235, http://dx.doi.org/10.1179/1743278215Y.0000000013.

Vigrass, L., Jessop, A., Brunskill, B. 2007. Regina Geothermal Project; *in* Summary of Investigations 2007, Volume 1, Saskatchewan Geological Survey, Sask. Industry Resources, Misc. Rep. 2007-4.1, CD-ROM, Paper A-2, 21 p.

Vilamajó E., 2016. CSEM monitoring at the Hontomín CO_2 Storage Site: modeling, experimental design and baseline results. Ph.D. Thesis, Facultat de Geologia, Universitat de Barcelona, Barcelona, Spain.

Vilamajó E., Queralt P., Ledo J., Marcuello A. 2013. Feasibility of monitoring the Hontomín (Burgos, Spain) CO_2 Storage Site using a deep EM Source. Surveys in Geophysics, 34, 441–461, https://doi.org/10.1007/s10712-013-9238-y.

Vilamajó, E., Rondeleux, B., Queralt, P., Marcuello, A., Ledo, J. 2015. A land controlled-source electromagnetic experiment using a deep vertical electric dipole: experimental settings, processing, and first data interpretation. Geophysical Prospecting 63, 1527-1540, doi: 10.1111/1365-2478.12331.

Vijanen, A., 2012. Description of the magnetospheric/ionospheric sources. In: Chave, A.D., Jones, A.G. (Eds.), The Magnetotelluric Method: Theory and Practice. Cambridge University Press, Cambridge (UK), ISBN 978-0521819275.

Vozoff, K., 1991. The magnetotelluric method. In: Nabighian, M.N. (Ed.), Electromagnetic Methods in Applied Geophysics – Volume 2 Applications. Society of Exploration Geophysicists, Tulsa, p. 641-711.

Wait, J.R., 1954. On the relation between telluric currents and the Earth's magnetic field. Geophysics 19, 281-289, https://doi.org/10.1190/1.1437994.

Ward, S.H., Hohmann, G.W., 1988, Electromagnetic Theory for Geophysical Applications; Chapter 4 in *Electromagnetic Methods in Applied Geophysics, Vol. I, Theory,* ed. Nabighian, M.N, Soc. Exploration Geophysicists, Tulsa, Okla, p. 131-311.

Wawrzyniak, P., Zlotnicki, J., Sailhac, P., Marquis, G., 2017. Resistivity variations related to the large March 9, 1998 eruption at La Fournaise volcano inferred by continuous MT monitoring. Journal of Volcanology and Geothermal Research 347, 185-206. https://doi.org/10.1016/j.jvolgeores.2017.09.011

Weckmann, U., Magunia, A., Ritter, O., 2005. Effective noise separation for magnetotelluric single site data processing using a frequency domain selection scheme. Geophysical Journal International, 161, 635-652.

West, G.F. Macnae, J.C., 1991. Physics of the electromagnetic induction exploration method. In: Nabighian, M.N. (Ed.), Electromagnetic Methods in Applied Geophysics – Volume 2 Applications. Society of Exploration Geophysicists, Tulsa, p. 5-45.

White, D.J., Roach, L.A.N., Roberts, B., Daley, T.M., 2014. Initial results from seismic monitoring at the

Aquistore CO2 storage site, Saskatchewan, Canada. Energy Procedia 63, 4418-4423, https://doi.org/10.1016/j.egypro.2014.11.477.

Whittaker, S., Worth, K. 2011. Aquistore: a fully integrated demonstration of the capture, transportation and geologic storage of CO_2. Energy Procedia, 4, 5607-5614, https://doi.org/10.1016/j.egypro.2011.02.550.

Wirianto, M., Mulder, W. A., Slob, E. C. 2010. A feasibility study of land CSEM reservoir monitoring in a complex 3-D model. Geophysical Journal International 181, 741-755, doi: 10.1111/j.1365-246X.2010.04544.x.

Worth, K., White, D., Chalaturnyk, R., Sorensen, J., Hawkes, C., Rostron, B., Johnson, J., Young, A., 2014. Aquistore project measurement, monitoring, and verification: from concept to CO_2 injection. Energy Procedia 63, 3202-3208, https://doi.org/10.1016/j.egypro.2014.11.345.

Zhdanov, M.S., Endo, M., Black, N., Spangler, L., Fairweather, S., Hibbs, A., Eiskamp, G.A., Will, R., 2013. Electromagnetic monitoring of CO_2 sequestration in deep reservoirs. First Break 31, 71-78.

Zhu, C., Hajnal, Z., 1993. Tectonic development of the northern Williston basin: a seismic interpretation of an east-west regional profile. Canadian Journal of Earth Sciences, 30, 621-630, https://doi.org/10.1139/e93-047.